Middle Pleistocene environments, landscapes and tephrostratigraphy of the Armenian Highlands: evidence from Bird Farm 1, Hrazdan Valley

Sherriff, J [1,2], Wilkinson, K. N[3], Harding, P[1], Hawkins, H[1] , Timms, R[1], Adler, D. S[4], Beverly, E[5], Blockley, S[1], Gasparyan, B[6], Manning, C[7], Mark, D[8], Nahapetyan, S[9], Preece, K[10]

1. Centre for Quaternary Research, Department of Geography, Royal Holloway, University of London, TW20 0EX, UK
2. Department of Geography, King's College London, WC2R 2LS, UK
3. Department of Archaeology, Anthropology and Geography, University of Winchester, Winchester SO22 4NR, UK
4. Department of Anthropology, University of Connecticut, Storrs, CT, USA
5. Department of Earth and Atmospheric Sciences, University of Houston, Houston, TX, USA
6. Institute of Archaeology and Ethnography, National Academy of Sciences of the Republic of Armenia, Yerevan, Armenia
7. Department of Earth Sciences, Royal Holloway, University of London, TW20 0EX, UK[
8. NERC Argon Isotope Facility, SUERC, Rankine Avenue, East Kilbride G75 0QF, UK
9. Yerevan State University, Yerevan, Armenia
10. Department of Geography, Faculty of Science and Engineering, Swansea University, Swansea, SA2 8PP, UK

Keywords: palaeoenvironments, Armenian Highlands, sedimentology, tephrostratigraphy, diatom analysis

Abstract

The significance of the southern Caucasus in understanding Pleistocene hominin expansions is well established. However, the palaeoenvironments in which Palaeolithic occupation of the region took place are presently poorly defined. The Hrazdan river valley, Armenian Highlands, contains a rich Palaeolithic record alongside Middle Pleistocene-aged volcanic, fluvial, and lacustrine strata, and thus offer exciting potential for palaeoenvironmental reconstruction. We present the first results of sedimentological, geochemical, tephrostratigraphical and biological (diatoms) study of the sequence of Bird Farm 1, located in the central part of the valley. These data show six phases of landscape development during the interval 440–200 ka. The sequence represents the first quantitative Pleistocene diatom record from the Armenian Highlands and the southern Caucasus, and indicates the persistence of a deep, stratified lacustrine system, with evidence for changing lake productivity that is tentatively linked to climate. Furthermore, major element chemical characterisation of visible and crypto-tephra horizons in the sequence enable the first stages of the development of a regional tephrostratigraphy. Together, the evidence from Bird Farm 1 demonstrates the importance of lacustrine archives in the region for palaeoenvironmental reconstruction and highlights the potential for linkages between archives on both a local and regional scale.

1. **Introduction**

The last three decades of archaeological research have established the southern Caucasus (defined here as the area of the Caucasus ecoregion [*sensu* Bailey 1989] lying south of the Greater Caucasus ridge) as an important region for the study of hominin evolution and expansion. Not only have hominin fossils dating to c. 1.8 Ma been found at Dmanisi, Georgia (Gabunia et al., 2000, Ferring et al., 2011, Lordkipanidze et al., 2013), the oldest known outside Africa, but at c. 320 ka, the earliest evidence of stone tool technology and hence cognitive developments that marked the beginning of the Middle Palaeolithic are evidenced at Nor Geghi 1 (NG1), Armenia (Adler et al., 2014). Further, sites in the region document Neanderthal and *Homo sapiens* occupations in a range of topographic and environmental settings before, during, and after the Middle to Upper Palaeolithic transition (e.g. Adler et al. 2006, 2008; Bar-Yosef et al., 2006; Golovanova et al., 2010; Pinhasi et al. 2011a, 2012; Gasparyan 2014; Moncel et al., 2015; Frahm et al. 2016; Pleurdeau et al., 2016; Tushabramishvili et al., 2012; Kandel et al. 2017; Glauberman et al. 2020a; Malinsky-Buller et al. 2020; Cullen et al. 2021). The archaeological record of the region is particularly significant given the southern Caucasus' contrasting topography, bedrock geology, climate and hence, vegetation - factors that must have provided both constraints and opportunities for the exploitation of the area by past hominin populations. Indeed, such limitations and possibilities would have been exaggerated in the Pleistocene given the magnitude and frequency of climate change, and the intensity of regional seismicity and volcanism. Nevertheless, despite the importance that climate and environment must have played in hominin occupation of the region - for example in determining the sub-regions that could be occupied, the seasonality of activity, resources available for subsistence – few palaeoenvironmental or palaeoclimate archives have been investigated beyond the level of the individual archaeological site (e.g. palynology at Hovk-1, Armenia and Dzudzuana, Georgia [Bar-Yosef et al., 2011; Pinhasi et al., 2008, 2011b]. In recent years, several studies focusing on landscape dynamics recorded by fluvial archives (e.g., Ollivier et al., 2016; Suchodoletz et al., 2016) and loess-palaeosol sequences (e.g., Wolf et al., 2016) have allowed inferences to be made regarding glacial-interglacial palaeoenvironmental change, while palaeoclimatic from some of these sequences has been derived from the study of *n*-alkane biomarkers (Trigui et al., 2019, Glauberman et al., 2020b) and molluscan assemblages (Ritcher et al., 2020). However, excepting Early Pleistocene palaeobotanical remains from lacustrine sequences from the Syunik region of southern Armenia (Joannin et al., 2010, Ollivier et al., 2010), data of regional palaeoenvironmental and palaeoclimate relevance are only presently available from areas adjacent to the southern Caucasus, i.e. from Lake Van in eastern Turkey (e.g. Litt and Anselmetti, 2014, Litt et al., 2014, Pickarski et al., 2015, Pickarski and Litt, 2017) and Lake Urmia in north-west Iran (Djamali et al., 2008). Given the heterogeneous geography of the area, it is debatable how far these Turkish and Iranian records are applicable to the southern Caucasus.

The Hrazdan valley, in central Armenia, has been a particular focus of Pleistocene geoarchaeological research, in part because its Palaeolithic record has been well documented since the Soviet era (see

Gasparyan et al., 2014). In the central part of the valley the river has incised a gorge that exposes volcanic, fluvial, and lacustrine strata. This suite of deposits is a product of the flow of mafic lavas along the valley from sources in the Aragats and Gegham volcanic massifs during the Lower and Middle Pleistocene, respectively. These lavas dammed the river leading to the formation of lakes in their lea, while subsequent downcutting of the River Hrazdan led to the breach of the dams and deposition of alluvium in the newly formed floodplain (Sherriff et al., 2019). A series of such volcanic-lacustrine-alluvial phases have been identified and dated from before c. 440 to c. 200 ka. Indeed, the association of terrigenous sediment, archaeological material and volcanic strata offers the possibility of preservation of palaeoenvironmental and palaeoclimate proxies in lacustrine deposits, precise dating of the archaeological and geological record by $^{40}Ar/^{39}Ar$, and tephrostratigraphic correlation between sites and sequences (Sherriff et al., 2019). Key amongst the sites demonstrating such potential is NG1, a locale from which >15,000 obsidian artefacts were recovered during excavations in 2008–2017, and which document the change from Lower to Middle Palaeolithic technologies (Adler et al., 2014; Frahm et al., 2020). NG1 is associated with alluvium and multiple palaeosols lying beneath both the youngest lava in the Hrazdan gorge (HGW-VI of Sherriff et al., 2019) and an underlying tephra $^{40}Ar/^{39}Ar$ dated to c. 308 ka (Adler et al., 2014), but biological proxies have not been preserved. However, a fossiliferous lacustrine and fluvial sequence beneath the same upper lava as found at NG1 exposure is located 1.35 km to the south-west of the NG1 at 'Bird Farm 1' (BF1). Here we report combined litho-, bio-, tephro- and chronostratigraphic data from BF1. Our aims in so doing are to (a) develop a model of climate and landscape change in the Hrzadan valley, (b) provide palaeoenvironmental context for hominin occupation at NG1, and (c) demonstrate the applicability of fragmentary lacustrine archives for improving our understanding of Middle Pleistocene environmental change in the Armenian Highlands and broader Caucasus region.

2. Geological and site context

BF1 (40˚ 20' 9.4" N, 44˚34' 53.1" E, 1388 m asl) is located c. 17 km north of Yerevan and is situated on the western side of the Hrazdan gorge, in the north-eastern Armenian Highlands (**Figure 1**). The surrounding mountains of the Gegham range reach elevations of 2304 m asl (Mt. Gutansar, 9.3 km north-east of BF1) and 2506 m asl (Mt. Hatis, 12.5 km east), while 14 km west of BF1, Mt. Arailer rises to 2604 m asl (Karapetyan and Adamyan, 1973). The large altitudinal variations mean that although characterised by a continental climate regime, average annual temperatures range from -4˚C to +21˚C, while there is a mean 400 mm of annual rainfall (Acopian Centre for the Environment, 2019).

The Armenian Highlands and the Caucasus (Greater and Lesser) mountain ranges mark the juncture of the Near East and Eurasia. Covering an area over 300,000 km^2, the Armenian Highlands is the southernmost of the mountain chains and borders the Iranian Plateau to the east, the Anatolian Plateau to the west, the Mesopotamian Plain to the south (Abich, 1845), while at its northern margin, the Armenia Highlands merge with the Lesser Caucasus. Both ranges were formed because of continental collision of the Arabian and

Eurasian plates from the Miocene onwards (Sosson et al., 2010). This tectonic activity also caused significant volcanic activity during the late Neogene and Quaternary, forming a range of volcanic landforms and strata which are clearly expressed across the region today (Sherriff et al., 2019; Halama et al., 2020 and references therein). BF1 lies within the NW margin of the Gegham volcanic massive (GVM) and close to the eastern margin of the Aragats volcanic massive (AVM). Locally, the AVM is represented by the Mt. Arailer stratovolcano, while Gutansar, Hatis and Mensakar, together with smaller features at Alapars (12.5 km north-west of BF1) and Fantan (11 km north-west), are the main volcanic centres of the western part of the GVM. Together, the edifices and associated volcanic deposits of Gutansar, Alapars and Fantan form the Gutansar Volcanic Complex (GVC).

The AVM and GVM are separated by the River Hrazdan, which flows NE–SW from Lake Sevan across the Hrazdan-Kotayk Plateau before draining into the River Araxes 18 km south of Yerevan. BF1 lies c. 0.6 km to west of the Hrazdan river and coincides with a lava plateau representing the western margin of the GVM. Lava flows emanating from Arailer terminate c. 0.7 km to the west of the site and at a 50 m higher elevation. The mode and chronology of volcanism of GVM and AVM volcanism has been described in detail elsewhere (Lebedev et al., 2011, 2013; Sherriff et al., 2019; Gevorgyan et al., 2020) and is only briefly reviewed here.

Previously published stratigraphies and chronologies of lava flows and pyroclastic deposits in the Hrazdan valley indicate that the area was subjected to several phases of volcanism during the Early and Middle Pleistocene. The earliest phase is associated with Arailer and the AVM between 1.40–0.65 Ma based on K-Ar and $^{40}Ar/^{39}Ar$ dating of lava flows and pyroclastic deposits in the vicinity of the Arailer edifice (Lebedev et al., 2011, Gevorgan et al., 2020). A combination of K-Ar, $^{40}Ar/^{39}Ar$ and Fission Track (FT) dating of volcanic formations associated with the NW sector of the GVM indicate a least four phases of volcanic activity between 700 and 200 ka (Karapetian et al., 2001; Lebedev et al., 2013; Sherriff et al., 2019). After 200 ka, the Hrazdan incised through the Lower–Middle Pleistocene volcanic strata, producing a c. 90 m deep gorge and exposing in section the lava flows associated with the GVM and, more rarely, sediment sequences interbedded between successive lava flows (Sherriff et al., 2019). These sequences have revealed a consistent pattern of lacustrine sedimentation succeeded by alluvial activity and then floodplain soil development (Frahm et al., 2017; Sherriff et al., 2019). BF1 is one such sequence.

BF1 directly underlies HGW-VI (Basalt 1; Adler et al., 2014; Sherriff et al., 2019), which is one of the youngest lava flows exposed in the Hrazdan gorge. This lava has a clear surface expression and is traceable along the western side of the Hrazdan valley, where it directly overlies HGW-IV (**Figure 1**), while chronological data for both lavas have been published from NG1 (Adler et al., 2014). Here a series of alluvial sediments incorporating several phases of pedogenesis, are interbedded between HGW-IV and HGW-VI, while $^{40}Ar/^{39}Ar$ dating has produced ages of 441 ± 6 ka and 197 ± 7 ka for HGW-IV and HGW-VI, respectively. $^{40}Ar/^{39}Ar$ dating of a volcanic ash unit in the uppermost stratum of the NG1 sequence (Unit 1), yielded an age of 308 ± 3 ka (Adler et al., 2014). Although HGW-IV is not visible in the locality of BF1, it is likely that BF1 and NG1 are at

least broadly contemporary given (i) a similar association with HGW-VI, (ii) both contain a comparable alluvial sequence overlying a lacustrine deposits (see below), and (iii) the two sites have a similar outcrop elevation (1402 m asl at NG1 and 1388 m asl at BF1).

3. Materials and methods

3.1. Fieldwork

The BF1 exposure was initially identified during a 2009 geomorphological survey. It comprises a 9 m high and 100 m long upstanding section exposed in the northern wall of a 'borrow pit' and is located immediately south of a chicken rearing facility (hence our 'Bird Farm' name for the site – the locale has no local toponym). The site has been revisited on several occasions (2011, 2013, 2015, 2017 and 2018) to excavate a test pit through to the base of the sequence, clean and describe the section, construct a formal log, and to sample the sequence for biostratigraphic and chronometric studies (**Figure 2**). The analyses reported below were carried out on contiguous 2cm-thick blocks of sediment taken through fine-grain strata and micromorphological study was conducted on 12 monolith samples collected in 120 x 60 mm stainless steel tins.

3.2. Bulk sedimentology, micromorphology and sediment geochemistry

Prior to laboratory analysis, the sediment subsamples were divided for separate bulk sedimentology/geochemical and tephrostratigraphic analyses. The sedimentology fraction was oven dried at 40˚C and then disaggregated. The dried samples were sieved at 2mm and the <2mm fraction retained for bulk sedimentological and geochemical analysis.

Mass-specific magnetic susceptibility (MS) was determined using a Bartington MS2 meter with MS2c dual frequency sensor at low (0.46 kHz) frequency (X^{lf}) following the protocol outline in Dearing (1999). Percentage organic content (%OC) and calcium carbonate content (%$CaCO_3$) were estimated from loss-on-ignition at 550˚C and 1000˚C respectively (Heiri et al., 2001). %$CaCO_3$ values were very low throughout the sequence (<2%) and so are not considered further. Particle size analysis was undertaken using a Malvern Mastersizer 3000 laser granulometer with a Hydro UM accessory following the protocol described in Glauberman et al. (2020b).

Micromorphology samples were prepared using standard impregnation techniques developed in the Centre for Micromorphology at Royal Holloway, University of London (Palmer et al., 2008). Thin sections were analysed using an Olympus BX-50 microscope with magnifications from 20x to 200x and photomicrographs were captured with a Pixera Penguin 600es camera. Thin section description followed terminology outlined in Bullock et al. (1985) and Stoops (2018).

Major and trace elemental concentrations of the <2mm bulk sediment samples were measured using Thermo Scientific Niton XL3 portable x-ray fluorescence analyser (pXRF) using the approach outlined by Glauberman et al. (2020b). The pXRF data in this study are used semi-quantitatively; however, it is worth noting that

several studies have demonstrated that measured elemental concentrations of bulk sediment samples using pXRF closely correspond to elemental concentrations derived from conventional XRF analysis (Roy et al., 2012, 2013).

3.4. Tephrostratigraphy

Sediment subsamples from the BF1 sequence were prepared for crypto-tephrostratigraphic analysis following standard density separation procedures (e.g. Blockley et al., 2015) and peaks in glass shard concentration were quantified following Geherels et al. (2008), using *Lycopodium* spiking to aid counting of high shard concentrations. Peaks in glass shard concentration were subsequently prepared for major and minor element chemical characterisation using density separation, but with the omission of the combustion stage to avoid thermal alteration (Pilcher and Hall, 1992; van den Bogaard and Schmincke, 2002). Individual volcanic glass shards were hand-picked onto silicon sheets and impregnated in an epoxy resin ready for chemical analysis (see Hall and Hayward 2014). In addition to the sediment samples, three visible tephra layers identified in the BF1 sequence (BF1-3, BF1-5 and BF1-7) were sampled as part of the contiguous sampling column and prepared following the methodology outlined above. Owing to the thickness and composition of BF1-3, a larger bulk sample from the unit was taken in addition to those from the sediment sampling column. This was processed by wet sieving a subsample of c. 2 g^{-1} through 250 µm and 125 µm meshes. The intermediary fraction was retained and prepared for chemical analysis in the same manner as the other glass shard samples.

Chemical analysis was undertaken on the three visible tephra layers identified in the field (BF1-3 [BF 142-144], BF1-5 [BF 122-124 and BF 124-126], BF1-7 [BF 46-48]) and on six peaks in glass shard concentrations as determined from the cryptotephra investigation (BF 154-156, BF 146-148, BF 116-118, BF 112-114, BF 104-106, BF 82-84) (**Figure 3**)**.** Resin stubs containing cryptotephras and visible ashes were carbon coated and analysed for major and minor elements using the WDS-EPMA (Cameca SX-100) facility at the University of Edinburgh. Probe conditions were guided by Hayward (2012). Calibration, precision and drift was assessed by the analysis of internal Lipari and BCR-2G secondary standards (**SI 1**).

3.5. Diatom analysis

Thirty-one sub-samples were prepared for diatom analyses from units BF1-6, BF1-7 and BF1-8 following the digestion procedure of Batterbee et al. (2001). Samples were studied at x1000 magnification using a Lecia DMBL. Identifications followed Krammer and Lange-Bertalot (1986, 1988, 1991a, 1991 b)**,** supplemented with Lange-Bertalot, (2001) and Krammer (2002) and was complemented by web-based resources (Spaulding et al., 2020) and Algaebase; (Guiry and Guiry, 2018).

4. Stratigraphy, sedimentology and geochemistry

4.1. Site stratigraphy

Ten stratigraphic units (BF1-1 to BF1-10) were identified in the BF1 sequence (**Figure 3, Table 1)**. Evident in the sequence is a mixture of volcanic (BF1-3, BF1-5, BF1-7, BF1-10), volcaniclastic (BF1-2, BF1-4) and siliclastic (BF1-6, BF1-8, BF1-9a-b) deposits while there is also evidence of the development of at least one palaeosol within BF1-9 (BF1-9b).

The lowermost unit (BF1-1) comprises massive poorly sorted sand-silt, but its base lies beneath the borrow pit floor and could not be found in the 2011 test pit. BF1-1 is overlain by horizontally laminated medium sand-silt and sand-silt sized volcanic ash (BF1-2), which, in turn is capped by massive, granular scoria lapilli (BF1-3). The overlying stratum comprises horizontally bedded coarse-fine sand with occasional granule-grade scoria lapilli (BF1-4), which in turn is capped by normally graded granule to coarse-silt grade scoria lapilli and ash (BF1-5). There is a sharp contact between BF1-5 and BF1-6, while the latter consists of well-sorted massive-laminated medium silt. BF1-6 is overlain by a massive, well sorted very coarse silt sized volcanic ash (BF1-7) which in turn is capped by a well-sorted massive-laminated medium silt (BF1-8). An unconformity represented by a sharp, undulating contact separates the fine-grained sequence outlined above, from predominantly coarse-grained clastic sediments. These are represented first by in BF1-9a, which comprises matrix-supported, trough cross- and planar-bedded, gravels of subrounded–rounded pebble and cobble-sized clasts in a coarse sand matrix. Within this unit are lenticular beds of laminated granules–coarse sands, and clasts are primarily of mafic lava, with lower frequencies of obsidian, intrusive igneous, metamorphic and sedimentary lithologies (**Table 1**). Also present within BF1-9 are intraclasts comprised of material derived from BF1-6 and/or BF1-8. BF1-9b conformably overlies BF1-9a and comprises clast and matrix supported gravels as described for the latter. However, the matrix of BF1-9b exhibits normal grading from coarse sand to sandy clay and is also formed of sub-angular aggregates with Fe/Mn oxide coatings and carbonate rhizoliths. Stage III carbonate coatings (*sensu* Gile, 1961) are present on gravel clasts. The BF1 sequence outlined above is capped by mafic lava (BF1-10) which thins to the east of the BF1 outcrop. BF1-10 has a blocky structure and rubbly base, while its upper surface is weathered and has developed a stage III carbonate crust. BF1-10 represents the local outcrop of HGW-VI in the Hrazdan valley stratigraphy and has been dated by $^{40}Ar/^{39}Ar$ at BF1 to 195 ± 8 ka and 198 ± 7 ka (Sherriff et al., 2019).

4.2. Bulk sedimentology

The results of the bulk sedimentological analyses undertaken on the <2 mm sediment size fraction indicate that the BF1-1 to BF1-8 deposits are moderately-poorly sorted and range in grain size from fine silt to very fine sand (**Figure 4**). X^{lf} values range from 0.34 to 94.69 $10^{-6}kg^{-1}m^3$ through the sequence, while organic carbon content (%OC) is low (<15%). However, there are clear trends in particle size distribution, X^{lf} and organic carbon content both between, but also within stratigraphic unit (%OC, **Figure 3**). BF1-1 has a moderately sorted medium silt grain size, low %OC and a relatively high X^{lf}. BF1-2 is characterised by lower X^{lf} compared to BF1-1, a low %OC and a slightly coarser grain size than the underlying unit. A shift to higher X^{lf} than that seen in BF1-1 and BF1-2, characterise BF1-3 to BF1-5, while these strata are also characterised

by low %OC. Variation in particle size distribution is evident through BF1-3 to BF1-5, with the <2mm fraction of BF1-3 principally comprising medium sand to granular ash and lapilli, while BF1-4 and BF1-5 are principally composed of coarse silt - very fine sand particles. A clear shift in all sedimentological parameters is observed at the BF1-5 to BF1-6 boundary, with BF1-6 characterised by relatively high %OC, low X^{lf} values and a generally finer particle size distribution than the underlying strata. There is also an observable increase in %OC in BF1-6 through the interval 7.92–7.62 m accompanied by a decrease in X^{lf}. BF1-7 marks a return to relatively high X^{lf} and low %OC, while grain size parameters indicate that the unit is a well sorted very coarse silt. BF1-9 has comparable sedimentological properties to BF1-6, with elevated %OC, low X^{lf} and a fine-medium silt grain size.

4.3. *Thin section micromorphology*

The main micromorphological properties of the BF1 deposits are presented in **Table 1**. Overall, the sequence is characterised by a high abundance of volcanic and siliclastic mineral fractions, with variations in the lithological and microstructural properties of these fractions evident between individual units.

At the microscale BF1-1 has a massive microstructure, with equal proportions of fine silt and volcanic ash matrix (**Figure 5a**). Mafic/felsic lithic fragments and feldspar mineral grains are present, while Fe/Mn oxide mottling of the matrix and Fe/Mn hypocoatings of voids are common. BF1-2 comprises grain- and matrix-supported, grain rich, normally graded laminae with sharp upper and lower boundaries **(Figure 5b)**. The matrix is principally of volcanic ash with some silt-grade clastic material, whilst grains are principally of volcanic lithologies. A loaded contact and enrichment of the matrix with clay is evident at the contact with BF1-3 (**Figure 5c**) and then the latter is characterised by a massive, grain-supported microstructure. Grains are exclusively of volcanic lithologies and comprise coarse silt to granular-sized scoria fragments, many of which have Fn/Mn hypocoatings. The same high frequency of volcanic material is observable at the microscale in the overlying BF1-4. This latter unit comprises alternations at irregular thicknesses of grain- and matrix-rich silt-sand particles with frequent volcanic ash and outsized mafic lithic fragments **(Figure 5d)**. Evident in the matrix are centric and pennate diatom frustules and amorphous organic material. BF1-5 has comparable textural and lithological properties to BF1-3 at the microscale, but evident towards the top of the former stratum is an increased abundance of clay in the micromorphology samples. This is expressed as the occurrence of stipple-striated β-fabric and clay coatings around grains **(Figure 5e)**. The upper boundary of BF1-5 is sharp and loaded, and also characterised by a high abundance of clay, with a clay rich matrix and clear horizontal parallel β-fabric. Clay infillings of scoria vesicles are also evident. Associated with the upper part of BF1-5 are frequent occurrences of organic matter (**Figure 5f**). This is represented by elongate fragments of organic material which are generally orientated sub-parallel to the unit bounding surface. Many fragments are Fe/Mn mottled.

A clear change in lithological components is recorded in the BF1-6 micromorphology samples. At the microscale, volcanic material is rare. The unit has a massive-weakly matrix rich microstructure comprising

fine-medium silt grade siliclastic material. Laminations are diffuse and represent irregular alternations of massive matrix-rich fine and medium silt. Mineral grains are rare and comprise medium silt size rounded quartz and feldspar (**Figure 5g**). Evident in the matrix are abundant diatom frustules which are a mixture of pennate, centric and acicular forms (**Figure 5h**). Also evident are amorphous algal filaments and organic fragments. Microstructural properties similar to BF1-6 are observed through BF1-8, albeit that the latter stratum is more grain rich than BF1-6, while Fe/Mn mottling of the matrix is evident towards the top of BF1-8.

4.4. Bulk sediment geochemistry

Figure 6 presents PCA results for selected major and minor elements (Al, Si, P, S, K, Ca, Ti, Fe, V, Cr Zn, Rb, Sr, Zr and Ba) in BF1-1 to BF1-8. PC1 represents 38.1% of variation in the bulk geochemical data, whilst PC2 accounts for 23.4%. Evident in the PCA are differential clustering of elements, while these are presented against select bulk sedimentological parameters (X^{lf}, %OC, and D_{50} PSA) in **Figure 6a**. Four groups of elements and sedimentological properties are identifiable: 1) Group A, characterised by high values of Si and %OC, 2) Group B, identified by high K, Rb and Nb values, 3) Group C, characterised by high values of V, Zr, Cr, Fe and Ti, and, 4) Group D, defined by Al, Sr, Ca, Zr and Ba and associated with high X^{lf} and D_{50} values

Sample scores for PC1 and PC2 are presented in **Figure 6b** which makes clear the clustering by stratigraphic unit in this dataset. The diatom-rich strata, BF1-6 and BF1-8, plot separately from the other units and are associated with elevated Group A element concentrations, whilst BF1-2, BF1-4, BF1-5 and BF1-7 are associated with the high Group B element concentrations. BF1-1 is associated with high values of Group C elements, whilst the scoria-rich unit, BF1-3, is associated with both high values of Group C and Group D elements, X^{lf} and D_{50}. These trends clearly show a strong lithological control on the geochemical signature on the BF1 deposits, with the clear differentiation of units comprised of volcanic and volcaniclastic particles (BF1-2, BF1-3, BF1-4 BF1-5, BF1-7) from those composed mostly of siliclastic material (BF1-1, BF1-6, BF1-8), while there is further differentiation of the volcanic and volcanoclastic units by broad geochemical composition.

Si/Al, Si/Ti, Si/K, Zr/Al and V/Cr ratios are plotted against stratigraphy in **Figure 7**. These ratios were selected as they give an indication of provenance (Muller et al., 2001; Kylander et al., 2013), the relative frequency of volcanic and siliclastic material (Martin-Puertas et al, 2011; Peti et al., 2020), and potential changes in biological productivity (Gill et al., 2011) within a single sedimentary sequence. Si/Al shows a clear pattern of relatively low ratios in units BF1-1 to BF1-5 and BF1-7, and elevated values associated in BF1-6 and BF1-8. In respect of the last it is further evident that there is an increase in the Si/Al ratio in the 7.85–7.62 m interval within BF1-6. A comparable trend to that seen in Si/Al is also observed in Si/K and Si/Ti, with the exception being BF1-3, which exhibits high Si/Ti values throughout the stratum. Zr/Al shows the converse trend, i.e. elevated ratios are found in association with BF1-1 to BF1-5 and BF1-7, with lower values occurring in BF1-6

and BF1-8. The lowest Zr/Al ratio is found in association with the interval 7.85–7.62 m. Although the dataset is characterised by a high degree of variability, especially in the lower strata, V/Cr ratios show a pattern of lower values associated with BF1-1, higher values in BF1-2 to BF1-5, and a shift back to lower values through BF1-6 to BF1-8. Elevated values of V/Cr are also recorded in the interval 7.85–7.62 m.

4.5. Sedimentological interpretation

Combined, the lithostratigraphical, bulk sedimentological, micromorphological and geochemical datasets from BF1 demonstrate clear shifts in depositional process through the sequence.

The fine and generally poorly sorted particle size distribution of BF1-1 is consistent with subaqueous sedimentation in a shallow water setting. Impregnative Fe/Mn features representative of leaching of Fe/Mn oxides under waterlogged conditions support such an interpretation (Lindo et al., 2010). A high proportion of both siliclastic and pyroclastic relative to biological material is consistent with high allochthonous inputs into the shallow-water setting, and is reflected in the high X^{lf} (Dearing, 1999). The sedimentological properties of BF1-2 are consistent with volcaniclastic deposition, while the occurrence of laminations of principally volcanic ash probably reflect the reworking as a primary tephra fall deposit. Lower X^{lf} values in this unit compared to BF1-1 are consistent with the high proportion of felsic igneous material evident at the microscale in this unit (Dearing, 1996). The presence of normally graded and massive laminations indicates subaqueous sediment delivery via sediment gravity flows into a shallow water body, with relative differences in particle size of the lamina reflecting variations in sediment supply and/or energy regime of these inwashing events (Stow and Bowen, 1980). The absence of significant alteration, breakage or rounding of the ash and lapilli fragments implies relatively local erosion and redeposition of pyroclastic material.

The earliest primary tephra fall deposit in BF1 is represented by BF1-3. Elevated X^{lf} values in this unit reflect the high proportion of ferrimagnetic igneous material (scoria and mafic lithic fragments), the absence of siliclastic material and a homogeneous microstructure. The relatively coarse and poorly sorted particle size distribution of BF1-3 may imply deposition from a proximal, rather than distal volcanic source (Pyle, 1989), while rapid sedimentation is suggested by load structures associated with the BF1-2 contact. A shift back to principally siliclastic sedimentation is recorded in BF1-4, where the presence of normally graded and massive laminations indicating the resumption of allochthonous sediment delivery via sediment gravity flows into a shallow lacustrine system (Lowe, 1982). The unit contains a high proportion of volcanic material, as indicated by high X^{lf} values through the unit and which is interpreted as reworking of BF1-3 tephra. The occurrence of diatom frustules in this unit indicates the first evidence of in-situ biological productivity at BF1.

A second primary tephra fall is represented by BF1-5, while the occurrence of clay in the part of the stratum indicates that the upper surface of the tephra has been weathered (Zehetner et al., 2003). Rapid *in situ* weathering and clay development is common in tephra that that been sub-aerially exposed (Bakker et al., 1996), and is associated with the alteration of lithic fragments and fragmentation of glass shards (Sedov et

al., 2010). Clay enrichment in BF1-5 is therefore interpreted as representing a shift from sub-aqueous to sub-aerial setting and subsequent exposure of the BF1-5 stratum to surface weathering processes. This conclusion is supported by the presence of organic fragments within BF1-5 which suggest that vegetation development and associated pedogenesis occurred at the former lake surface.

BF1-6 indicates the resumption of lacustrine sedimentation. Collectively, BF1-6 and BF1-8 represent the occurrence of fine-grained, diatomaceous clastic sediment deposition, while laminations indicate accretion in a deep, stratified water body. Allochthonous inputs are represented by the occurrence of silt-grade clastic particles, while variation between laminations is driven by shifts in the energy of input (Kemp, 1996). These structures are consistent with sediment delivery via sediment gravity flows, while rounded grains indicate the occurrence of some aeolian inputs (Kalińska and Nartišs, 2014). A significant autochthonous biogenic component is indicated by enhanced organic content and the abundance of diatoms. The absence of significant changes in lithological properties through BF1-6 and BF1-8 indicates an interval of quiescent conditions that is in contrast with the underlying lacustrine strata. The only discernible changes through BF1-6 and BF1-8 are an increase in organic content and corresponding reduction in X^{lf}. These latter are interpreted as reflecting an increase in the autochthonous biogenic input associated with enhanced productivity and/or decreased catchment erosion and therefore clastic input. BF1-6 and BF1-8 are separated by the third primary volcanic unit in the BF1 sequence (BF1-7). The fine-grained and well sorted nature of BF1-7 suggests a primary ash deposited via suspension through the lake water column.

BF1-9 is separated from the underlying strata by an unconformity, the latter marking the shift from fine- to coarse-grained clastic sedimentation. The trough and planar bedforms of the gravels and sands of BF1-9 are consistent with deposition in a moderate energy fluvial system and likely represent lateral accretion of a braided river system (Reineck and Singh 1980; Miall, 1996). Clast lithologies are diverse, reflecting the wide range of geological strata present in the Hrazdan valley (Kharazyan, 2005; Sherriff et al, 2019). BF1-9b represents the pedogenic modification of the fluvial gravels, with the presence of carbonate and textural pedofeatures representing compound Bk1, Bk2, Bk3, BCk, Ck horizons forming within the alluvial parent material subsequent to the cessation of fluvial activity at the site. The absence of a defined A-horizon suggests that BF1-9b was truncated by the passage of the mafic lava (BF1-10) that caps the BF1 sequence.

Variations in the sedimentological properties of the BF1-1 sequence are evident in the bulk geochemistry of the deposits (**Figure 6**). The clustering of strata by elemental groups (A-D) indicates a strong lithological control on the sequence. The diatomaceous units, BF1-6 and BF1-8 are found in association with elevated values of Si and high organic content (Group A), both of which are indicators of autochthonous biogenic content. Variations between elemental groups B and C probably reflect the different contributions of felsic (characterised by higher values of Rb, K and Nb) and mafic (high values of V, Zn, Fe, Cr and Ti) volcanic material in the BF1 sequence. BF1-7 and BF1-2 closely plot with Group B elements, representing a high abundance of felsic volcanic ash in these units, while the fine-grained lacustrine unit BF1-4, also plots with

Group B elements, indicating the reworked volcanic component evident in thin section. The scoria-rich volcanic deposits (BF1-3 and BF1-5) are associated with elevated values of Group C elements, reflecting their mafic origin. BF1-3 and BF1-5 also occur in association with high values of Group D elements. Interpretation of a single origin of Group D is problematic, given that it contains a suite of elements associated with clastic and volcanic inputs. Nevertheless, elevated values of Group D elements in BF1-3 and BF1-5 likely reflect the elemental composition of the felsic and mafic volcanic material that comprise these units. Conversely, elevated concentrations of Group D elements in the fine-grained siliclastic unit BF1-1, are probably a product of the allochthonous inputs of detrital clastic and volcanic material within this stratum.

Lithological variations are also clearly expressed in the Si/Al, Si/Ti, Si/K, Zr/Al and V/Cr ratios (**Figure 7**). Evident from these latter, however, are also changes within strata, specifically BF1-6, where an increase in Si relative to Ti, K and K is observed 7.85–7.62 m, with an associated increase in V/Cr ratio values and decrease in Zr/Al ratio values. The interpretation of the Si profile through BF1-6 and BF1-8 is that it is reflecting a predominately autochthonous biogenic signal, whilst Al, K and Ti are reflecting contributions of detrital clastic and volcanic material. Consequently, the peak in Si relative to Al, K and Ti likely reflects either increased diatom productivity or a change in diatom composition in this interval, resulting in higher biogenic silica loadings (Martin-Puertas et al., 2011). Zr/Al ratios frequently are used for a proxy for aeolian sedimentation in lacustrine settings, given Zr is concentrated in more mobile sand-silt fraction of clastic sediment in respect to Al (Huang et al., 2003; Roy et al., 2006; 2009). Although the Zr/Al relationship is complicated by the concentration of Zr in mafic volcanic minerals (Roy et al., 2009, and as demonstrated by high Zr/Al ratio in BF1-3), evident in the interval 7.85–7.62 m is a decrease in Zr relative to Al in comparison to both the lower part of BF1-6 and BF1-8. This could tentatively be interpreted as a reduction in aeolian input into the lake system, occurring contemporaneously with increased biological activity. V/Cr is used as an indicator for lake anoxia, as V preferentially precipitates under anoxic conditions, whilst Cr remains relatively immobile in both anoxic and oxic settings (Schaller et al., 1997; Das et al., 2009). Higher V/Cr ratios values therefore may imply the persistence of anoxic conditions, possibly associated with enhanced thermal stratification or more eutrophic conditions. These shifts occur at the same interval as an increase in organic content and increased concentrations of benthic diatoms, suggesting that these geochemical signals are representing changes in lake productivity.

5. Tephrostratigraphy

5.1. Tephrostratigraphy results

Volcanic glass shard concentrations are high throughout the BF1 sequence, ranging from a few thousand to several million shards g^{-1} (**Figure 3; S1).** The majority of the glass shards extracted from the BF1 record are colourless, blocky and amorphous with numerous flutes and some open and closed vesicles. The surface texture on some specimens, particularly the cryptotephra, is pitted and uneven, while some specimens also

exhibit cracking, all features suggestive of post-depositional alteration and hydration (Blockley et al., 2005). Samples from BF1-3 comprise blocky glass shards of a distinct greenish-yellow/ brown colour and rich in mineral inclusions. Alongside these were colourless shards similar to those found throughout the rest of the sequence (described above).

5.2. Tephra chemistry and correlation

Chemical classification diagrams for the visible tephra layers (BF1-3 [BF 142-144], BF1-5 [BF 122-124 and BF 124-126], BF1-7 [BF 46-48]) and peaks in glass shard concentrations as determined from the cryptotephra investigation (BF 154-156, BF 146-148, BF 116-118, BF 112-114, BF 104-106, BF 82-84) are presented in **Figure 8.** The full major and minor element dataset is available and summary data are presented in **S1.** The colourless shards identified in BF1-3 (BF 142-144_b) as well as the glass shards recovered from the visible tephra BF1-5 (BF 122-124_a and BF 124-126_a) and BF1-7 (BF 46-48), and the cryptotephra intervals (BF 154-156_a, BF 146-148, BF 116-118, BF 112-114, BF 104-106, BF 82-84), all exhibit a High-K calc-alkaline rhyolitic signature that based on TAS classification alone , are chemically indistinguishable (**Figure 8**). These tephra show considerable overlap with other calc-alkaline centres from central Turkish volcanic sources, e.g. Acıgöl, Erciyes Dağ, Göllü Dağ, and Hasan Dağ (commonly referred to as the Central Anatolian Volcanic Province [CAVP]). However, the BF1 rhyolites may be tentatively distinguished from these, with plots of Al_2O_3 and TiO_2 wt.% proving particularly useful (**Figure 8**). Single grain glass chemistry available from Armenian volcanic centres is limited, but analyses obtained as part of wider investigations by the authors suggest that the most consistent chemical overlap with the BF1 rhyolites are those obtained from volcanic deposits mapped to the Gutansar Volcanic Complex (GVC, **Figure 8**). Given the proximity of Gutansar to BF1 (**Figure 1A**) and the abundance of glass shards identified within the studied sequence, it is most probable that the BF1 rhyolitic shards correlate to an eruptive episode(s) from this centre. However, the present limited knowledge with regards the geochemistry of regional eruptive products, precludes any firmer proposals regarding an exact source or timing of eruption(s) at present.

Alongside the primary population in BF1-5 (BF 124-126_a) are two further data clusters, denoted here as b and c populations. Population b has marginally higher TiO_2 values (c. 0.29 wt%), whereas population c has lower SiO_2 values (65-69 wt%) and higher Al_2O_3 (c. 17.7 wt%) compared to the primary population. It has not been possible to identify a chemical correlative of these analyses which likely reflects the incompleteness of the regional glass chemical dataset.

Glass shards comprising Population a in BF1-3 (BF 142-144_a) and a single analysis from BF1-5 (BF 124-126_d) can be classified as trachyandesite (**Figure 8**). Volcanic centres in the GVM are known to have produced trachyandesitic volcanic products during the Pleistocene (Arutyunyan et al. 2007; Lebedev et al. 2013), as

have centres located in eastern Turkey (commonly referred to as the Eastern Anatolian Volcanic Province [EAVP] in recent scientific literature, e.g. Pearce et al., 1990; Yilmaz et al., 1998; Sumita and Schmincke 2013a, b; Lebedev et al., 2016a, b) and possibly the Syunik Highlands in southern Armenia (Kandel et al., 2017). Given their relative proximity to BF1, these volcanic regions are amongst the most probable sources for BF1-3 (BF 142-144_a) and BF1-5 (BF 124-126_d). Single grain glass shard analyses are either not yet available from the intermediate products of the aforementioned regions, or are available in very low quantities, and whilst data is available from what is hypothesised to represent volcanic products from the Syunik Highlands (Kandel et al., 2017), this link has not been proven chemically. At present, the greatest chemical similarity to BF1-3 (BF 142-144_a) and BF1-5 (BF 124-126_d) is exhibited by a tephra identified within Kalavan-2, a Middle Palaeolithic site c. 60 km NE of BF1 (Malinsky-Buller et al., 2021). However, the age of the Kalavan-2 site means that it is too young to be a correlative of BF1, and it has not yet been possible to directly provenance the Kalavan tephra. Given the thickness of the BF1-3 and BF1-5 tephra horizons, their relatively coarse grain size, and the probable correlation of the rhyolitic tephra at BF1 to Gutansar, we argue it is most likely that BF1-3 (BF 142-144_a) and BF1-5 (BF 124-126_d) also originated from the proximal GVC.

6. Diatom analysis

6.1. Diatom results

A summary of the diatom assemblage is presented in **Figure 9 a**nd the full dataset is included in **S2.** BF1-6 8.29–8.00 m is dominated by fluctuating levels of *Stephanodiscus medius* Håkansson and *Aulacoseira granulata* (Ehrenberg) Simonsen, with low but persistent occurrences of Narviculoid taxa. At 8.00 m, diatom concentrations fall, and thereafter remain low, with limited species diversity, until c. 7.85 m at which point concentrations of all diatom taxa rise notably. *A. granulata* initially dominates at 7.85 m, *S. medius* peaks at 7.70-7.65 m, there are first appearances of *Staurosirella pinnata* (Ehrenberg) Williams and Round, *Cocconeis placentula* spp. Ehrenberg and *Pseudostaurosira* species at 7.85m, while Narviculoid taxa also increase in concentration. In BF1-7 (7.60-7.56 m) all diatom concentrations are reduced because of the dilution of the sediment by volcanic ash discussed above. However, concentrations return to higher levels above 7.55 m, with *S. medius* dominating the assemblage between 7.54 and 7.33 m (BF1-8), while *A. granulata* occurs in lower, but consistent levels. *Pseudostaurosira* species are also present in consistent, but low quantities, while *S. pinnata* and *C. placentula* spp. initially occur in lower concentrations than 7.85–7.65 m before increasing above 7.32 m.

6.2. Diatom interpretation

The diatom record indicates that the strata formed in a deep, temperate, alkaline lake, with high nutrient availability (Rioual et al., 2007), the latter likely linked to a high concentration of incorporated silicic tephra shards. Variations in the dominance between the two key species, *S. medius* and *A. granulata*, are likely linked to variations in length and timing of spring and autumn lake overturning, with *S. medius* thriving during episodes of intense and prolonged springtime mixing (Bradbury et al., 2002; Rioual et al., 2007). In contrast

the heavily silicified *A. granulata* requires warmer temperatures, alongside deep mixing, to keep the heavily silicified taxa in the photic zone and is thus often found in lakes with strong autumn overturning. Both species require nutrient rich waters (Kilham et al., 1986; O'Farrell et al., 2001), and they often appear to track one another, with high concentrations indicating periods of intensified spring and autumn overturning, both of which allow nutrient resuspension (Winder and Hunter, 2008), and hence a reduced period of summer stratification. Evident through the lower part of BF1-6 is a relatively consistent diatom assemblage indicating lake stability, with limited changes in lake stratification regime and/or physicochemical properties of the water column. A notable shift in the diatom assemblage is evident at 7.85 m, represented by a significant increase in the occurrence of benthic taxa above this depth. Two possible mechanisms could explain the change: 1) an extension of the euphotic zone, favouring benthic diatom production (Wolin and Duthie, 1999), or 2) a change in lake productivity or biodiversity, resulting in an increase in benthic diatom productivity (Althouse et al., 2014; Leira et al., 2015). The continued presence of a relatively high proportion of benthic taxa through the upper part of BF1-6 and BF1-8 represents the continuation of relative lake stability, albeit associated with differing lake conditions.

7. Landscape and environmental change at Bird Farm 1 and in the Hrazdan valley

The sequence at BF1 provides evidence for changes in both lacustrine sedimentation and depositional environment in the Hrazdan gorge during the Middle Pleistocene. Broadly, the sequence represents two phases of deposition during which there were three primary tephra falls, the basal two separated from the upper by an interval of sub-aerial exposure. The second phase of lacustrine sedimentation is followed by a period of alluvial activity and pedogenesis prior to the capping of the sequence by lava emplacement (**Table 2**). As outlined in Section 2, a broad chronology for landscape development at BF1 is provided by $^{40}Ar/^{39}Ar$ ages estimates derived from the lava flow (BF1-11) that caps the deposits and lava flows HGW-VI and HGW-IV outcropping at NG1. It is important to note that attempts were made to $^{40}Ar/^{39}Ar$ date the visible tephras BF1-3 and BF1-7 as part of this study. Extraction of minerals (feldspar) followed the protocol outlined in Adler et al. (2014); however, it was not possible to obtain the required number of crystals of an appropriate size for accurate $^{40}Ar/^{39}Ar$ dating. However, the age of the BF1 sequence can be further refined by correlation of the deposits with those at NG1 (**Figure 10**). $^{40}Ar/^{39}Ar$ dating of sanidines derived from the upper sediment stratum (Unit 1) at NG1 have yielded an age of 308 ka, while that layer in turn directly overlies a series of pedogenically modified alluvial deposits (NG1 Units 2–5). We argue that the latter are floodplain and levee facies of the same stream that deposited the BF1-9 channel sediments. Accepting this hypothesis would imply that the BF1 sequence accumulated in the 440–308 ka interval, with pedogenic development at BF1 occurring contemporaneously with NG1 during MIS 9e. Given the correlation of the upper alluvial strata at BF1 to MIS 9e we hypothesise lake persistence at BF1 is associated with an earlier interval of warmer conditions, possibly during MIS 11.

516 The earliest phase of lacustrine sedimentation (BF1-1 to BF1-5) is associated with the development of a
517 shallow lacustrine system after 440 ka. Lake formation likely occurred as a response to impeded drainage in
518 the Hrazdan basin and due to damming of the palaeo-Hrazdan by lava flow emplacement (Sherriff et al.,
519 2019). Associated with this phase were at least three intervals of volcanic activity, represented by the two
520 visible primary airfall deposits (BF1-3 and BF1-5) and the reworked felsic ash within BF1-2. The particle size
521 distribution and close chemical similarity with proximal deposits from the GVM, suggest that a local volcanic
522 centre (e.g., Gutansar), is the likely source of the primary and reworked tephra. Together, the presence of a
523 high volume of volcanic material and allochthonous siliclastic sediment in the lower strata of the BF1
524 sequence indicates a highly dynamic landscape in which large volumes of easily erodible material lay on the
525 land surface surrounding the basin. Consequently, the lacustrine system was subject to a high amount of
526 inwashing and rapid sediment deposition.

527 The second phase of landscape evolution at BF1 is represented by the weathered upper stratum of BF1-5,
528 indicating a reduction in water level in the lacustrine system, sub-aerial weathering of the tephra, with clay
529 illuviation. Formation of this surface represents a depositional hiatus in the BF1 sequence. The cause of the
530 change in water level is, however, not clear from the sedimentary evidence alone. It may in part be a
531 consequence of infilling the basin through the rapid deposition of volcanic material. Alternatively, it could
532 represent a reduction in water level as a response to climatic (aridity) or, more likely, geomorphic processes
533 related to damming of the lake elsewhere in the catchment (Sherriff et al., 2019).

534 The third phase of landscape evolution recorded in the BF1 sequence is represented by a return to lacustrine
535 sedimentation, albeit associated with a deeper, stratified water body. It is likely that this new lake system
536 formed because of the damming of the palaeo-Hrazdan downstream of the BF1 locale. The formation of a
537 deep lake system involves: a) the presence of a basin of a significant depth to contain the waterbody (e.g., a
538 valley) and b) a significant inflow of water. By implication it was likely that there was not a barrier to palaeo-
539 Hrazdan flow upstream of the BF1 locale at this time. Sedimentological, geochemical and diatom evidence
540 indicate the persistence of a deep, stratified lake with periodic seasonal overturning in a warm climate. This
541 indicates lake persistence under relatively stable environmental conditions, with allochthonous inputs
542 principally from aeolian sources and periodic in-washing events. At least one primary pyroclastic airfall event
543 is recorded during the interval (BF1-7), which given the chemical similarity of this ash unit to the tephra in
544 the rest of the sequence, may indicate a GVM eruptive source, although Turkish eruptive sources (e.g., the
545 CAVP) cannot be excluded.

546 The combined diatom and geochemical evidence from the BF1 sequence indicates at least one interval of
547 changing lake conditions during this third phase. This change was manifested by an increase in benthic
548 diatom taxa occurring contemporaneously with enhanced organic content and Si production, a relative
549 reduction in allochthonous inputs and a greater level of anoxia. Together, these lines of evidence suggest an
550 extension of the euphotic zone, resulting in enhanced lake productivity and a shift in lake trophic status

(Althouse et al., 2014; Leira et al., 2015). There a several possible explanations for this: 1) a reduction in lake level as a consequence of climatic change (enhanced warming and/or aridity) or geomorphic processes resulting in the extension and development of aquatic vegetation (e.g., Ruhland et al., 2015), 2) a reduction in lake turbulence as a consequence of falling wind strength, favouring the development of benthic diatom communities (e.g., Wang et al., 2012) or, 3) a reduction in the duration or change in timing of ice-cover, enhancing light availability and nutrient availability.

The fourth phase of landscape evolution in the BF1 locale represents the onset of alluvial deposition, characterised by the moderate energy in-channel fluvial sedimentation. Given the unconformity between the alluvial sediments and underlying lacustrine strata, it is not clear when this activity occurred. Nevertheless, we can hypothesize that that the depositional shift to a fluvial style was likely a consequence of breaching of the dam downstream of the BF1 locale, resulting in drainage of the lake system and the commencement of fluvial activity and floodplain development in the Hrazdan valley. The gravels forming the BF1 fluvial deposits have a diverse lithology, representing the wide range of Quaternary and Pre-Quaternary geologies outcropping in the modern Upper Hrazdan valley (Sherriff et al., 2019), indicating that the fluvial system (likely the palaeo-Hrazdan) had a comparable catchment to the modern Hrazdan. This interval of alluvial activity was followed by soil development on the palaeo-Hrazdan floodplain, which likely occurred alongside the development of climax vegetation communities in MIS9e. The final phase of Pleistocene landscape evolution recorded at BF1 is lava emplacement, this latter representing the final period of effusive volcanic activity affecting the Hrazdan gorge at 200 ka (MIS 7). Previous mapping of this lava flow indicates that it originated from either the Gutansar, Hatis or Menaksar edifices located on the eastern side of the Hrazdan valley (Sherriff et al., 2019).

8. Discussion

8.1. Palaeoenvironmental significance of the Bird Farm sequence

The combined sedimentological, geochemical and diatom evidence from BF1 provide a record of environmental conditions during the Middle Pleistocene. There is evidence for two phases of sediment accumulation under temperate conditions, albeit associated with differing depositional regimes, and at least four intervals of changing hydrological conditions in the Hrazdan Basin around the BF1 locale. Significantly, the BF1 record provides the first quantitative diatom evidence for changing environmental conditions in the Armenian Highlands (and the wider southern Caucasus) during the Middle Pleistocene.

Given the chronology of the site, we hypothesize that the temperate conditions recorded at BF1 represent separate interglacial periods, MIS 9e and MIS 11c. The former is represented by the development of mature Bk horizons, indicating floodplain soil formation and probably associated with the development of climax vegetation communities under fully interglacial conditions, whilst the latter is represented by the persistence of a deep lake system under warm temperatures. Significantly, shifts observed during this interval of lake persistence may hint at changes in temperature or precipitation regime *within* MIS 11. Whilst we are keen

586 to avoid over-interpretation given ambiguities in elucidating the driver(s), and timing of this shift, the
587 evidence highlights the potential of lacustrine systems for recording sub-Milankovitch environmental
588 changes in the southern Caucasus.

589 The prevalence of warm and humid interglacial conditions in the Hrazdan valley during the Middle
590 Pleistocene supports the limited palaeoenvironmental evidence from the region. Malacological evidence
591 from loess-palaeosol sequences in northern Armenia indicates the development of forest steppe during
592 interglacials indicating increased humidity and warm temperatures in comparison with semi-arid to arid
593 conditions during glacial periods (Richter et al., 2020). These sites lie at a much lower elevation (c. 400 m
594 asl) than the Hrazdan valley. However, pollen evidence from Lake Van, which is at a comparable altitude to
595 the Hrazdan valley (1647 m asl), albeit 180 km to the south-west and separated from BF1 by the Armenian
596 Highlands, also indicates enhanced warmth and increased humidity during Middle Pleistocene interglacials
597 as evidenced by the development of mixed-oak steppe (Litt et al., 2014).

598 The hydrological changes recorded in the BF1 sequence cannot be interpreted on the basis of climate alone,
599 given the strong geomorphic and volcanic control on the Hrazdan valley throughout the Pleistocene (Sherriff
600 et al., 2019). Rather, these hydrological changes are hypothesised to be linked to changing sediment supply
601 and impeded drainage of the palaeo-Hrazdan upstream and downstream of the BF1 locale, both of which are
602 closely related to the volcanic history of the basin. Indeed, the evidence from BF1 supports the broad
603 sediment succession recorded elsewhere in the Hrazdan valley of lava emplacement damming the Hrazdan
604 valley and lake formation, a shift to fluvial deposition as a function of breaching of the lava dam or base level
605 change, floodplain development and subsequent lava emplacement. Evident in the BF1 sequence, however,
606 is more complexity in the pattern of geomorphic change, with evidence for the occurrence of two distinct
607 lake systems in the Hrazdan gorge during the interval 440–200 ka. Whilst it is not possible from the
608 geomorphic evidence to account for the causes of these changes, it does imply changes to the pattern of the
609 drainage of the palaeo-Hrazdan on at least two occasions prior to the onset of fluvial deposition at the BF1
610 locale.

611 *8.2. Tephrostratigraphical significance of the Bird Farm sequence*

612 The BF1 sequence records the first Middle Pleistocene tephrostratigraphy to be published from the Armenian
613 Highlands. Evident in the sequence are three stratigraphically distinct tephra layers each representing
614 separate eruptive events/phases, while there are also high concentrations of cryptotephra throughout.
615 Overlapping chemical signatures of the cryptotephra, supported by micromorphology and sedimentological
616 evidence, suggests that the record represents the local reworking of volcanic deposits derived from the GVM.
617 High background concentration of volcanic glass in the sequence therefore acts to mask any primary tephra
618 deposition, meaning distinct eruptive episodes are unlikely to be identified in the cryptotephra record.

The visible tephra in the BF1 sequence therefore provides the best means for tephrostratigraphic correlation. Major element glass chemistry of these tephra indicates potential eruptive sources in Turkey and the GVM. However, given the thickness of the BF1-3, BF1-5 and BF1-7 tephra horizons, a local source is favoured. Radiometric (K-Ar) and FT dating of obsidian and other felsic deposits proximal to the edifice of Gutansar provides an estimated interval of activity between 550 and 200 ka (Oddone et al., 2000; Badalian et al., 2001; Karapetian et al., 2001; Lebedev et al., 2011; 2013), overlapping with the formation of the BF1 sequence (440–200. ka). However, we cannot currently exclude other volcanic centres in the western GVM (e.g., Hatis and Menaksar) given that they also have eruptive phases spanning this Middle Pleistocene interval (Badalian et al., 2001; Karapetian et al., 2001; Lebedev et al., 2013) while their glass chemistry is at present incompletely resolved.

Potential correlations of the visible tephra in the BF1 sequence, and indeed other Pleistocene sequences from the Armenian Highlands and broader Caucasus region (e.g., Malinsky-Buller et al., 2021), with known source areas is more problematic for three reasons: 1) the chemical similarity of tephras derived from different local and regional volcanic sources on the basis of their major element chemistry, 2) incomplete understanding of the timing and chemical signature of eruptions from local volcanic centres in Armenia, specifically those in the GVM and AVM, which have chronologies indicating eruptive episodes during the Pleistocene (Chernyshev et al., 2002; Lebedev et al., 2011; Meliksetian et al., 2014)), and 3) the absence of single-shard glass data from distal volcanic centres that also have eruptive histories spanning the Middle Pleistocene (e.g., Elbrus [Greater Caucasus], Damavand [Iranian Plateau] Nemrut, Suphan Tendurek [eastern Turkey]). Despite these uncertainties, the tephrostratigraphy at BF1 offers considerable potential for the correlation of sediment sequences within the Hrazdan Valley and beyond. Indeed, such isochrons will be of particular significance if they can be linked to tephras associated with archaeological sites (e.g., Kagshi 1; Sherriff et al., 2019; lower strata in NG1, Adler et al., 2014). Specifically, the tephrostratigraphic correlation of archives that contain palaeoenvironmental proxy evidence, such as BF1, will allow for the future development of a framework linking landscape, environmental and archaeological changes in the Armenian Highlands and the southern Caucasus as a whole.

8.3. Bird Farm and the Hrazdan valley archaeological record

The BF1 sequence cannot yet be firmly correlated with hominin activity at NG1 or indeed elsewhere, a situation that will persist until either tephra-derived isochrons can be established or absolute ages are obtained for the BF1 tephras (either directly by $^{40}Ar/^{39}Ar$ or indirectly by chronologies derived elsewhere). However, on the assumption that the fluvial channel strata at BF1 (BF1-9) are facies equivalents of the floodplain deposits at NG1 (Units 1–4), it can in turn be inferred that the lacustrine beds at BF1 are lateral equivalents of lake sediment outcropping beneath the alluvial layers at NG1 (**Figure 10**) (Adler and Wilkinson

652 unpublished data). Further, acceptance of such an inference would imply that the lake stretched at least 1.7
653 km north-eastwards from the BF1 locale. It is also of note that the earliest Palaeolithic artefacts at NG-1 are
654 associated with rubble derived from the 440 ka HGW-IV lava, while lake sediments have formed around the
655 trachyandesite cobbles and boulders (Adler and Wilkinson unpublished data). These data have significant
656 implications for the interpretation of the initial hominin activity at NG1 that will be considered elsewhere,
657 but suffice to say that lake margin settings were utilised by hominin groups throughout the Early and Middle
658 Pleistocene (e.g., Blumenschine et al., 2012; Roach et al., 2016; Stewart et al., 2020). They are recognised
659 as ecotonal environments that allow both freshwater and adjacent terrestrial settings to be exploited, while
660 at the same time being a location for the congregation of potential prey. Indeed, the high nutrient status of
661 the BF1 lake suggests that it would have been a rich source of aquatic resources, particularly during its deep-
662 water phase. At a broader level, the posited BF1–NG1 correlation would confirm previously published
663 suggestions that Lower and early Middle Palaeolithic occupations in the Caucasus region are archaeologically
664 most visible during interglacials (Adler et al., 2014; Sherriff et al., 2019), periods which, as discussed above,
665 are argued to have been warm and humid. Even so, excepting NG1 and Koudaro III in South Ossetia
666 (Doronichev, 2011), Palaeolithic sites in the region have yet to be chronometrically dated to the MIS 11–9
667 interval, albeit that several are known from the MIS 7 interglacial (e.g. Azokh cave in Nagorno Karabakh
668 [Fernández Yalvo et al., 2010; Asyran et al., 2014] and Djruchula, Georgia [Mercier et al., 2010]). The
669 tephrostratigraphic approach outlined above may in the future enable correlation of the BF1 stratigraphy
670 with the wider Middle Pleistocene archaeological record.
671
672 **9. Conclusions**

673 - The Bird Farm-1 sequence represents the first record for the Armenian Highlands that combines
674 sedimentological, tephrostratigraphical and diatom data in order to reconstruct Middle Pleistocene
675 environmental and landscape change in the region.
676 - We have demonstrated six phases of landscape development in the Hrazdan gorge between
677 successive lava flow emplacements at 440 and 197 ka and comprising the development of at least
678 two distinct lacustrine systems, separated by an interval of sub-aerial weathering. Deposition in a
679 lacustrine setting was followed by an interval of fluvial activity and subsequent land surface stability.
680 Within the sequence is evidence for at least two intervals of sediment accumulation under warm
681 conditions, which , on the basis of the Hrazdan valley stratigraphy (Sherriff et al., 2019), we
682 hypothesize to be MIS 9e and MIS 11c.
683 - Diatom data from the sequence provide evidence for fluctuating lake conditions during one of these
684 intervals and which might be linked to changing climate regimes within a single warm phase. Whilst
685 further proxy evidence is needed to fully understand these changes, the record demonstrates the
686 strong potential for fragmentary lake sequences (such as BF1) in the Caucasus region to record
687 Middle Pleistocene climatic changes. This result is of particular significance in a region where highly

dynamic tectonism means that the likelihood of finding long, continuous lacustrine sequences spanning large parts of the Pleistocene is low.

- Major element chemical characterisation of three visible tephra and six cryptotephra horizons in the sequence represents the first published stage in the development of a regional tephrostratigraphy for the Middle Pleistocene. The chemistry of the visible tephra horizons suggests derivation from Armenian and Turkish sources. Whilst combined stratigraphical, chronological and glass shard geochemical evidence from two of these tephras allows for the tentative correlation to proximal deposits of the GVM volcano, Gutansar, c. 10 km NE of the site.
- Together, the diatom and tephra evidence demonstrate that linkages can be established between palaeoenvironmental archives at both a local (Hrazdan valley) and regional (Armenian Highlands and Caucasus) scale. Such connections will enable us to better understand the environmental backdrop of the expansion, behavioural change, and evolution of Middle Pleistocene hominins in the region generally.

Acknowledgements

The authors would like to thank Dr Khachatur Meliksetian (Director of the Institute of Geological Sciences, RA Academy of Sciences) and Dr Dmitri Arakelyan (Institute of Geological Sciences, RA Academy of Sciences), Dr Pavel Avetisyan (Director of the Institute of Archaeology and Ethnography, RA Academy of Sciences) and Karen Bayramyan (Head of the Protection of Monuments of History and Culture Agency for the Ministry of Culture, Republic of Armenia), for their insights on the archaeology and geology of central Armenia and for logistical help. We are also very grateful to Suren Kesejian for his invaluable assistance in the field and elsewhere, and the Partevian family for hosting us during fieldwork. Dr Monika Knul (University of Winchester), Jayson Gill (University of Connecticut), Alexander Brittingham (University of Connecticut), Yannick Raczynsky-Henk and Dr Phil Glauberman are also thanked for their help in the field. Finall,y we thank two anonymous reviewers for their constructive comments on an earlier version of the paper. The analyses and a significant part of the fieldwork reported here was funded by the Leverhulme Trust (RPG-2016-102), while the University of Connecticut's Norian Armenian Programs Committee and the Gfoeller Renaissance Foundation, USA, also provided financial assistance.

References

Abich, G., 1845. *Über die geologische Natur des Armenischen Hochlandes*. Druck von Heinrich Laakmann, Dorpat.

Acopian Center for the Environment, 2019. Vector Database Armenia. American University of Armenia. http://www.acopiancenter.am/GISPortal/ (Accessed 16/02/2021).

Adler, D.S., Bar-Oz, G, Belfer-Cohen, A., Bar-Yosef, O., 2006. Ahead of the game: Middle and Upper Palaeolithic hunting practices in the Southern Caucasus. *Current Anthropology* 47(1), pp. 89–118.

Adler, D.S., Bar-Yosef, O., Belfer-Cohen, A., Tushabramishvili, N., Boaretto, E., Mercier, N., Valladas, H., Rink, W.J., 2008. Dating the demise: Neanderthal extinction and the establishment of Modern Humans in the Southern Caucasus. *Journal of Human Evolution* 55(5), pp. 817–833.

Adler, D.S., Wilkinson, K.N., Blockley, S., Mark, D.F., Pinhasi, R., Schmidt-Magee, B.A., Nahapetyan, S., Mallol, C., Berna, F., Glauberman, P.J., Raczynski-Henk, Y., 2014. Early Levallois technology and the Lower to Middle Paleolithic transition in the Southern Caucasus. *Science*, 345 (6204), pp.1609-1613.

728 Asryan, L., Oilé, A., Moloney, N., King, T., 2014. Lithic assemblages of Azokh Cave (Nagorno Karabagh, Lesser
729 Caucasus): Raw materials, technology and regional context. *Journal of Lithic Studies*, 1 (1), pp.33–54.

730 Althouse, B., Higgins, S., Vander Zanden, M.J., 2014. Benthic and planktonic primary production along a
731 nutrient gradient in Green Bay, Lake Michigan, USA. *Freshwater Science*, 33 (2), pp.487-498.

732 Arutyunyan, E.V., Lebedev, A.V., Chernyshev, I.V., Sagatelyan, A.K., 2007. Geochronology of Neogene–
733 Quaternary volcanism of the Geghama Highland (Lesser Caucasus, Armenia). *Doklady Earth Sciences* ,416,
734 pp. 1042–1046.

735 Bailey, R.G., 1989. *Bailey Ecoregions Map of the Continents*. World Conservation Monitoring Center,
736 Cambridge. https://www.unep-wcmc.org/resources-and-data/baileys-ecoregions-of-the-world.

737 Bakker, L., Lowe, D.J., Jongmans, A.G., 1996. A micromorphological study of pedogenic processes in an
738 evolutionary soil sequence formed on Late Quaternary rhyolitic tephra deposits, North Island, New
739 Zealand. *Quaternary International*, 34, pp.249-261.

740 Bar-Yosef, O., Belfer-Cohen, A., Adler, D.S., 2006. The Implications of the Middle-Upper Paleolithic
741 chronological boundary in the Caucasus to Eurasian Prehistory. *Anthropologie* XLIV(1), pp. 81–92.

742 Bar-Yosef, O., Belfer-Cohen, A., Mesheviliani, T., Jakeli, N., Bar-Oz, G., Boaretto, E., Goldberg, P., Kvavadze,
743 E., Matskevich, Z., 2011. Dzudzuana: an Upper Palaeolithic cave site in the Caucasus foothills
744 (Georgia). *Antiquity*, 85 (328), pp.331-349.

745 Battarbee, R., Juggins, S., Gasse, F., Anderson, N., Bennion, H., Cameron, N., Ryves, D., Pailles, C., Chalie, F.,
746 Telford, R., 2001. An Information System for Palaeoenvironmental Reconstruction. *EDDI* 81, 1–94.

747 Blockley, S.P.E., Pyne-O'Donnell, S.D.F., Lowe, J.J., Matthews, I.P., Stone, A., Pollard, A.M., Turney, C.S.M.,
748 Molyneux, E.G. 2005. A new and less destructive laboratory procedure for the physical separation of distal
749 glass tephra shards from sediments. *Quaternary Science Reviews,* 24, 1952–1960.

750 Blumenschine, R.J., Masao, F.T., Stollhofen, H., Stanistreet, I.G., Bamford, M.K., Albert, R.M., Njau, J.K.,
751 Prassack, K.A., 2012. Landscape distribution of Oldowan stone artifact assemblages across the fault
752 compartments of the eastern Olduvai Lake Basin during early lowermost Bed II times. *Journal of Human*
753 *Evolution*, 63 (2), pp.384-394.

754 Bradbury, P., Cumming, B., Laird, K., 2002. A 1500-year record of climatic and environmental change in Elk
755 Lake, Minnesota III: Measures of past primary productivity, *Journal of Paleolimnology*, 27, 321–340.

756 Bullock, P., Fedoroff, N., Jongerius, A., Stoops, G. and Tursina, T., 1985. *Handbook for soil thin section*
757 *description*. Waine Research.

758 Cullen, V.L., Smith, V.C., Tushabramishvili, N., Mallol, C., Dee, M., Wilkinson, K.N., Adler, D.S. (2021) A revised
759 AMS and tephra chronology for the Late Middle to Early Upper Paleolithic occupation of Ortvale Klde,
760 Republic of Georgia. *Journal of Human Evolution,* 151, 102908.

761 Das, S.K., Routh, J., Roychoudhury, A.N., Klump, J.V., Ranjan, R.K., 2009. Phosphorus dynamics in shallow
762 eutrophic lakes: an example from Zeekoevlei, South Africa. *Hydrobiologia*, 619 (1), pp.55-66.

763 Dearing, J.A., 1999. Magnetic susceptibility, In: Walden, J., Oldfield, F., Smith, J. (Eds.), Environmental
764 Magnetism; a practical guide. Quaternary Research Association Technical Guide No. 6, London

765 Dearing, J.A., Dann, R.J.L., Hay, K., Lees, J.A., Loveland, P.J., Maher, B.A., O'grady, K., 1996. Frequency-
766 dependent susceptibility measurements of environmental materials. *Geophysical Journal International*, 124
767 (1), pp.228-240.

768 Djamali, M., de Beaulieu, J.L., Shah-hosseini, M., Andrieu-Ponel, V., Ponel, P., Amini, A., Akhani, H., Leroy,
769 S.A., Stevens, L., Lahijani, H., Brewer, S., 2008. A late Pleistocene long pollen record from Lake Urmia, NW
770 Iran. *Quaternary Research*, 69 (3), pp.413-420.

771 Fernández-Jalvo, Y., King, T., Yepiskoposyan, L., Andrews, P., (Eds.), 2016. *Azokh Cave and the Transcaucasian*
772 *Corridor*. Vertebrate Paleobiology and Paleoanthropology Series. Springer, Dordrecht.

773 Ferring, R., Oms, O., Agusti, j., Berna, F., Nioradze, M., Shelia, T., Tappen, M., Vekua, A., Zhvania, D.,
774 Lordkipanidze, D., 2011. Earliest human occupations at Dmanisi (Georgian Caucasus) dated to 1.85–1.78 Ma.
775 *Proceedings of the National Academy of Sciences*, 108, pp. 10432–10436.

776 Frahm, E., Feinberg, J.M., Schmidt-Magee, B.A., Wilkinson, K.N., Gasparyan, B., Yeritsyan, B., Adler, D.S.,
777 2016. Middle Palaeolithic Toolstone Procurement Behaviors at Lusakert Cave 1, Hrazdan Valley, Armenia.
778 *Journal of Human Evolution*, 91, pp. 73–92.

779 Frahm, E., Jones, C.O., Corolla, M., Wilkinson, K.N., Sherriff, J.E., Gasparyan, B., Adler, D.S., 2020. Comparing
780 Lower and Middle Palaeolithic lithic procurement behaviors within the Hrazdan basin of central
781 Armenia. *Journal of Archaeological Science: Reports*, 32, p.102389.

782 Frahm, E., Sherriff, J., Wilkinson, K.N., Beverly, E.J., Adler, D.S., Gasparyan, B., 2017. Ptghni: A new obsidian
783 source in the Hrazdan River basin, Armenia. *Journal of Archaeological Science: Reports*, 14, pp.55-64.

784 Gabunia, L., Antón, S., Lordkipanidze, D., Vekua, A., Justus, A., Swisher, C., 2001. Dmanisi and dispersal.
785 *Evolutionary Anthropology*, 10, pp. 158–170.

786 Gasparyan, B., Egeland, C.P., Adler, D.S., Pinhasi, R.M Glauberman, P., Haydosyan, H. 2014. The Middle
787 Paleolithic occupation of Armenia: summarizing old and new data. In Gasparyan, B. and Arimura, M. (Eds.)
788 *Stone Age of Armenia*. Center for Cultural Resource Studies, Kanazawa University, pp.65–106.

789 Gehrels, M.J., Newnham, R.M., Lowe, D.J., Wynne, S., Hazell, Z.J., Caseldine, C. 2008. Towards rapid assay of
790 cryptotephra in peat cores: review and evaluation of various methods. *Quaternary International*, 178, 68-84.

791 Gevorgyan, H., Breitkreuz, C., Meliksetian, K., Israyelyan, A., Ghukasyan, Y., Pfänder, J.A., Sperner, B., Miggins,
792 D.P., Koppers, A., 2020. Quaternary ring plain-and valley-confined pyroclastic deposits of Aragats
793 stratovolcano (Lesser Caucasus): Lithofacies, geochronology and eruption history. *Journal of Volcanology and*
794 *Geothermal Research*, 401, p.106928.

795 Gile, L.H., 1961. A classification of Ca horizons in soils of a desert region, Dona Ana County, New Mexico. *Soil*
796 *Science Society of America Journal*, 25 (1), pp.52-61.

797 Gill, J.L., Williams, J.W., Jackson, S.T., Donnelly, J.P., Schellinger, G.C., 2012. Climatic and megaherbivory
798 controls on late-glacial vegetation dynamics: a new, high-resolution, multi-proxy record from Silver Lake,
799 Ohio. *Quaternary Science Reviews*, 34, pp.66-80.

800 Glauberman, P., Gasparyan, B., Sherriff, J., Wilkinson, K., Li, B., Knul, M., Brittingham, A., Hren, M.T.,
801 Arakelyan, D., Nahapetyan, S., Raczynski-Henk, Y., 2020b. Barozh 12: formation processes of a late Middle
802 Paleolithic open-air site in western Armenia. *Quaternary Science Reviews*, 236, p.106276.

803 Glauberman, P., Gasparyan, B., Wilkinson, K.N., Frahm, E., Nahapetyan, S., Arakelyan, D., Raczynski-Henk, Y.,
804 Haydosyan, H., Adler, D.S., 2020. Late Middle Paleolithic technological organisation and behaviour at the
805 open-air site of Barozh 12 (Armenia). *Journal of Paleolithic Archaeology*, 3, pp.1095–1148.

806 Golovanova, L.V., Doronichev, V.B., Cleghorn, N.E., Koulkova, M.A., Sapelko, T.V. Shackley, M.S., 2010.
807 Significance of ecological factors in the Middle to Upper Paleolithic Transition. *Current Anthropology* 51(5),
808 pp.655–688.

Guiry, M.D., Guiry, G.M., 2018. AlgaeBase. World-wide electronic publication [WWW Document]. URL http://www.algaebase.org (Accessed 09/08/20).

Halama, R., Meliksetian, K., Savov, I.P., Sugden, P.J., Sokół, K., 2020. Pinched between the plates: Armenia's voluminous record of volcanic activity. *Geology Today*, 36 (3), pp.101-108.

Hall, M. and Hayward, C. 2014. Preparation of micro-and crypto-tephras for quantitative microbeam analysis. *Geological Society, London, Special Publications* 398, 21-28.

Heiri, O., Lotter, A.F., Lemcke, G., 2001. Loss on ignition as a method for estimating organic and carbonate content in sediments: reproducibility and comparability of results. *Journal of paleolimnology*, 25 (1), pp.101-110.

Huang J, Kang S, Zhang Q, Guo J, Chen P, Zhang G, Tripathee L. 2013. Atmospheric deposition of trace elements recorded in snow from the Mt. Nyainqêntanglha region, southern Tibetan Plateau. *Chemosphere*, 92(8),pp. 871–881

Joannin, S., Cornée, J.J., Münch, P., Fornari, M., Vasiliev, I., Krijgsman, W., Nahapetyan, S., Gabrielyan, I., Ollivier, V., Roiron, P., Chataigner, C., 2010. Early Pleistocene climate cycles in continental deposits of the Lesser Caucasus of Armenia inferred from palynology, magnetostratigraphy, and $^{40}Ar/^{3}9Ar$ dating. *Earth and Planetary Science Letters*, 291 (1-4), pp.149-158.

Kalińska, E. and Nartišs, M., 2014. Pleistocene and Holocene aeolian sediments of different location and geological history: A new insight from rounding and frosting of quartz grains. *Quaternary International*, 328, pp.311-322.

Kandel, A.W., Gasparyan, B., Allué, E., Bigga, G., Bruch, A.A., Cullen, V.L., Frahm, E., Ghukasyan, R., Gruwier, B., Jabbour, F., Miller, C.E., 2017. The earliest evidence for Upper Paleolithic occupation in the Armenian Highlands at Aghitu-3 Cave. *Journal of human evolution*, 110, pp.37-68.

Karapetian, S.G., Jrbashian, R.T., Mnatsakanian, A.Kh. 2001. Late collision rhyolitic volcanism in the north-eastern part of the Armenian Highland. *Journal of Volcanology and Geothermal Research*. 112, pp. 189–220.

Karapetyan, K.I., Adamyan A.A., 1973. *Noveyshiy vulkanizm nekotorikh rayonov Armyanskoy SSR (Younger volcanism of some regions of the Armenian SSR)*. Armenian Academy of Sciences Publishing House, Yerevan (in Russian).

Kemp, A.E.S. 1996. Laminated sediments as paleo-indicators, In A.E.S. Kemp (Ed.), Palaeoclimatology and Palaeoceanography from Laminated Sediments, Geol. Soc. Spec. Publ, 116 pp. vii-xii

Kharazyan H. 2005. Geological map of Republic of Armenia. In: Kharazyan, H, editor. Ministry of nature protection of Republic of Armenia [Internet]. Ministry of Nature Protection of Republic of Armenia, Yerevan

Kilham, P., Kilham, S.S., Hecky, R.E., 1986. Hypothesized resource relationships among African planktonic diatoms. *Limnology and Oceanography,* 31, 1169–1181.

Krammer, K. and Lange-Bertalot, H., 1986. Bacillariophyceae. 1: Teil: Naviculaceae., Süßwasserf. ed. Gustav Fischer Verlag, Stuttgart, New York.

Krammer, K. and Lange-Bertalot, H., 1988. Bacillariophyceae. 2: Teil: Bacillariaceae, Epithmiaceae, Surirellaceae., Süßwasserf. ed. Gustav Fischer Verlag, Stuttgart, New York.

Krammer, K. and Lange-Bertalot, H., 1991a. Bacillariophyceae. 3: Teil: Centrales, Fragilariaceae, Eunotiaceae., Süßwasserf. ed. Gustav Fischer Verlag, Stuttgart, Jena.

Krammer, K. and Lange-Bertalot, H., 1991b. Bacillariophyceae. 4: Teil: Achnanthaceae., Süßwasserf. ed. Gustav Fischer Verlag, Stuttgart, Jena.

Krammer, K., 2002. Diatoms of Europe. Diatoms of the European Inland Waters and Comparable Habitats. Volume 3: Cymbella. Germany.

Kylander, M.E., Klaminder, J., Wohlfarth, B., Löwemark, L., 2013. Geochemical responses to paleoclimatic changes in southern Sweden since the late glacial: the Hässeldala Port lake sediment record. *Journal of Paleolimnology*, 50 (1), pp.57-70.

Le Bas, M.J., Le Maitre, R.W., Streckeisen, A. and Zanettin, B (1986) 'A chemical classification of volcanic rocks based on the total alkali-silica diagram' Journal of petrology 27, (3) 745-750

Lange-Bertalot, H., 2001. Diatoms of Europe: Diatoms of the Europe inland waters and comparable habitats. Volume 2: Navicula sensu stricto, 10 Genera separated from Navicula sensu lato, Frustulia. ed. Germany.

Lebedev, V.A., Chernyshev, I.V., Shatagin, K.N., Bubnov, S.N., Yakushev A.I. 2013. The Quaternary volcanic rocks of the Geghama Highland, Lesser Caucasus, Armenia: geochronology, isotopic Sr–Nd characteristics, and origin. *Journal of Volcanology and Seismology*, 7, pp. 204–229.

Lebedev, V.A., Chernyshev, I.V., Yakushev, A.I. 2011 The initiation time and the duration of Quaternary magmatism in the Aragats neovolcanic area, Lesser Caucasus, Armenia, *Doklady Earth Sciences*, 437, pp. 808–812.

Lebedev, V.A., Chugaev, A.V., Ünal, E., Sharkov, E.V., Keskin, M. 2016b. Late Pleistocene Tendürek Volcano (Eastern Anatolia, Turkey). II. Geochemistry and petrogenesis of the rocks. *Petrology* 24, 234-270.

Lebedev, V.A., Sharkov, E.V., Ünal, E., Keskin, M. 2016a. Late Pleistocene Tendürek volcano (Eastern Anatolia, Turkey): I. Geochronology and petrographic characteristics of igneous rocks. *Petrology* 24, 127-152.

Leira, M., Filippi, M.L., Cantonati, M., 2015. Diatom community response to extreme water-level fluctuations in two Alpine lakes: a core case study. *Journal of Paleolimnology*, 53 (3), pp.289-307.

Lindbo, D.L., Stolt, M.H., Vepraskas, M.J., 2010. Redoximorphic features. In Stoops, G., Marcelino, V. and Mees, F. eds., 2010. *Interpretation of micromorphological features of soils and regoliths*. Elsevier.

Litt, T. and Anselmetti, F.S., 2014. Lake Van deep drilling project PALEOVAN. *Quaternary Science Reviews*, 104, pp.1-7.

Litt, T., Pickarski, N., Heumann, G., Stockhecke, M., Tzedakis, P.C., 2014. A 600,000 year long continental pollen record from Lake Van, eastern Anatolia (Turkey). *Quaternary Science Reviews*, 104, pp.30-41.

Lordkipanidze, D., de León, M.S.P., Margvelashvili, A., Rak, Y., Rightmire, G.P., Vekua, A., Zollikofer, C.P., 2013. A complete skull from Dmanisi, Georgia, and the evolutionary biology of early Homo. *Science*, *342* (6156), pp.326-331.

Lowe, D.R., 1982. Sediment gravity flows; II, Depositional models with special reference to the deposits of high-density turbidity currents. *Journal of sedimentary research*, 52 (1), pp.279-297.

Malinsky-Buller, A., Glauberman, P., Wilkinson, K.N., Li, B., Frahm, E., Gasparyan, B., Timms, R., Adler, D.S., Sherriff, J. (2020). Evidence for Middle Palaeolithic occupation and landscape change in central Armenia at the open-air site of Alapars-1. *Quaternary Research*, 99, 223-247.

Malinsky-Buller, A., Glauberman, P., Ollivier, V., Lauer, T., Timms, R., Frahm, E., Brittingham, A., Triller, B., Kindler, L., Knul, M.V. and Krakovsky, M., 2021. Short-term occupations at high elevation during the Middle Paleolithic at Kalavan 2 (Republic of Armenia). PloS one, 16(2), p.e0245700.

Martín-Puertas, C., Valero-Garcés, B.L., Mata, M.P., Moreno, A., Giralt, S., Martínez-Ruiz, F., Jiménez-Espejo, F., 2011. Geochemical processes in a Mediterranean Lake: a high-resolution study of the last 4,000 years in Zonar Lake, southern Spain. *Journal of Paleolimnology*, 46 (3), pp.405-421

Miall, A.D. 1996. *The Geology of Fluvial Deposits.* Springer. Berlin.

Moncel, M.-H., Pleurdeau, D., Pinhasi, R., Yeshurun, R., Agapishvili, T., Chevalier, T., Lebourdonnec, F.-X., Poupeau, G., Nomade, S., Jennings, R., Higham, T., Tushubramishvili, N., Lordkipanidze, D., 2015. The Middle Palaeolithic record of Georgia: a synthesis of the technological, economic and paleoanthropological aspects. *Anthropologie* LIII, pp.93–125.

Murray, J., Domínguez-Alonso, P., Fernández-Jalvo, Y., King, T., Lynch, E.P., Andrews, P., Yepiskoposyan, L., Moloney, N., Cacères, I., Allué, E., Asryan, L., Ditchfield, P., Williams, D.M., 2010. Pleistocene to Holocene stratigraphy of Azokh 1 cave, Lesser Caucasus. *Irish Journal of Earth Sciences*, 28, pp. 75–91.

Müller, J., Oberhänsli, H., Melles, M., Schwab, M., Rachold, V., Hubberten, H.W., 2001. Late Pliocene sedimentation in Lake Baikal: implications for climatic and tectonic change in SE Siberia. *Palaeogeography, Palaeoclimatology, Palaeoecology*, 174 (4), pp.305-326.

O'Farrell, I., Tell, G., Podlejski, A., 2001. Morphological variability of Aulacoseira granulata (Ehr.) Simonsen (Bacillariophyceae) in the Lower Parana River (Argentina). *Limnology* 2, 65–71.

Ollivier, V., Nahapetyan, S., Roiron, P., Gabrielyan, I., Gasparyan, B., Chataigner, C., Joannin, S., Cornée, J.J., Guillou, H., Scaillet, S., Munch, P., 2010. Quaternary volcano-lacustrine patterns and palaeobotanical data in southern Armenia. *Quaternary International*, *223*, pp.312-326.

Ollivier, V. Fontugne, M., Lyonnet, B., Chataigner, C. 2016. Base level changes, river avulsions and Holocene human settlement dynamics in the Caspian Sea area (middle Kura valley, South Caucasus). *Quaternary International* 395, 79-94.

Pearce, J.A., Bender, J.F., De Long, S.E., Kidd, W.S.F., Low, P.J., Güner, Y., Saroglu, F., Yilmaz, Y., Moorbath, S., Mitchell, J.G. 1990. Genesis of collision volcanism in Eastern Anatolia, Turkey. *Journal of Volcanology and Geothermal Research* 44, 189-229.

Peccerillo, A. and Taylor, S.R. 1976. 'Geochemistry of Eocene calc-alkaline volcanic rocks from the Kastamonu area, northern Turkey' Contributions to mineralogy and petrology 58, (1) 63-81

Peinerud, E.K., 2000. Interpretation of Si concentrations in lake sediments: three case studies. *Environmental Geology*, 40 (1-2), pp.64-72.

Peti, L., Gadd, P.S., Hopkins, J.L., Augustinus, P.C., 2020. Itrax μ-XRF core scanning for rapid tephrostratigraphic analysis: a case study from the Auckland Volcanic Field maar lakes. *Journal of Quaternary Science*, 35 (1-2), pp.54-65.

Pickarski, N. and Litt, T., 2017. A new high-resolution pollen sequence at Lake Van, Turkey: insights into penultimate interglacial–glacial climate change on vegetation history. *Climate of the Past*, 13 (6), pp.689-710.

Pickarski, N., Kwiecien, O., Djamali, M., Litt, T., 2015. Vegetation and environmental changes during the last interglacial in eastern Anatolia (Turkey): a new high-resolution pollen record from Lake Van. *Palaeogeography, Palaeoclimatology, Palaeoecology*, 435, pp.145-158.

Pilcher, J.R. and Hall, V.A., 1992. Towards a tephrochronology for the Holocene of the north of Ireland. *The Holocene*, 2 (3), pp.255-259.

Pinhasi, R., Gasparyan, B., Nahapetyan, S., Bar-Oz, G., Weissbrod, L., Bruch, A.A., Hovsepyan, R., Wilkinson, K., 2011b. Middle Palaeolithic human occupation of the high altitude region of Hovk-1, Armenia. *Quaternary Science Reviews*, 30 (27-28), pp.3846-3857.

Pinhasi, R., Gasparyan, B., Wilkinson, K., Bailey, R., Bar-Oz, G., Bruch, A., Chataigner, C., Hoffmann, D., Hovsepyan, R., Nahapetyan, S., Pike, A.W.G., 2008. Hovk 1 and the Middle and Upper Paleolithic of Armenia: a preliminary framework. *Journal of Human Evolution*, 55 (5), pp.803-816.

Pinhasi, R., Higham, T.F., Golovanova, L.V., Doronichev, V.B., 2011a. Revised age of late Neanderthal occupation and the end of the Middle Paleolithic in the northern Caucasus. *Proceedings of the National Academy of Sciences*, 108 (21), pp.8611-8616.

Pinhasi, R., Nioradze, M., Tushabramishvili, N., Lordkipanidze, D., Pleurdeau, D., Moncel, M.H., Adler, D.S., Stringer, C. and Higham, T.F.G., 2012. New chronology for the Middle Palaeolithic of the southern Caucasus suggests early demise of Neanderthals in this region. *Journal of Human Evolution*, 63 (6), pp.770-780.

Pleurdeau, D., Moncel, M.-H., Pinhasi, R., Yeshurun, R., Higham, T., Agapishvili, T., Bokeria, M., Muskhelishvili, A., Le Bourdonnec, F.-X., Nomade, S., Poupeau, G., Bocherens, H., Frouin, M., Genty, D., Pierre, M., Pons-Branchu, E., Lordkipanidze, D., Tushabramishvili, N., 2016. Bondi Cave and the Middle-Upper Palaeolithic transition in western Georgia (south Caucasus). Quaternary Science Reviews, 146, pp.77–98.

Pyle, D.M., 1989. The thickness, volume and grainsize of tephra fall deposits. *Bulletin of Volcanology*, *51*(1), pp.1-15.

Reineck H.-E., Singh I.B. 1975. *Depositional Sedimentary Environments*, Springer, Berlin

Roach, N.T., Hatala, K.G., Ostrofsky, K.R., Villmoare, B., Reeves, J.S., Du, A., Braun, D.R., Harris, J.W.K., Behrensmeyer, A.K., Richmond, B.G., 2016. Pleistocene footprints show intensive use of lake margin habitats by Homo erectus groups. *Scientific Reports*, 6, 26374.

Richter, C., Wolf, D., Walther, F., Meng, S., Sahakyan, L., Hovakimyan, H., Wolpert, T., Fuchs, M., Faust, D. 2020. New insights into Southern Caucasian glacial–interglacial climate conditions inferred from Quaternary gastropod fauna. J*ournal of Quaternary Science,* 35, 634–649

Rioual, P., Andrieu-Ponel, V., de Beaulieu, J.-L.L., Reille, M., Svobodova, H., Battarbee, R.W., 2007. Diatom responses to limnological and climatic changes at Ribains Maar (French Massif Central) during the Eemian and Early Würm. *Quaternary Science Reviews,* 26, 1557–1609.

Roy, P.D., Jonathan, M.P., Pérez-Cruz, L.L., Sánchez-Córdova, M.M., Quiroz-Jiménez, J.D., Romero, F.M., 2012. A millennial-scale L ate Pleistocene–Holocene palaeoclimatic record from the western Chihuahua Desert, Mexico. *Boreas*, 41 (4), pp.707-718.

Roy, P.D., Nagar, Y.C., Juyal, N., Smykatz-Kloss, W., Singhvi, A.K., 2009. Geochemical signatures of Late Holocene paleo-hydrological changes from Phulera and Pokharan saline playas near the eastern and western margins of the Thar Desert, India. *Journal of Asian Earth Sciences*, *34*(3), pp.275-286.

Roy, P.D., Rivero-Navarette, A., Lopez-Balbiaux, N., Pérez-Cruz, L.L., Metcalfe, S.E., Sankar, G.M. , Sánchez-Zavala, J.L., 2013. A record of Holocene summer-season palaeohydrological changes from the southern margin of Chihuahua Desert (Mexico) and possible forcings. *The Holocene*, *23*(8), pp.1105-1114.

965 Roy, P.D., Smykatz-Kloss, W., Sinha, R., 2006. Late Holocene geochemical history inferred from Sambhar and
966 Didwana playa sediments, Thar Desert, India: comparison and synthesis. *Quaternary International*, 144 (1),
967 pp.84-98.

968 Schaller, T., Moor, H.C. and Wehrli, B., 1997. Sedimentary profiles of Fe, Mn, V, Cr, As and Mo as indicators
969 of benthic redox conditions in Baldeggersee. *Aquatic sciences*, 59 (4), pp.345-361.

970 Schmitt, A.K., Danišík, M., Evans, N.J., Siebel, W., Kiemele, E., Aydin, F. and Harvey, J.C., 2011. Acigöl rhyolite
971 field, Central Anatolia (part 1): high-resolution dating of eruption episodes and zircon growth rates.
972 *Contributions to Mineralogy and Petrology*, *162*(6), pp.1215-1231.
973
974 Sedov, S., Stoops, G., Shoba, S. 2010 Regoliths and soils on volcanic ash, in
975 G. Stoops, V. Marcelino, F. Mees (Eds.), Interpretation of Micromorphological Features of Soils and
976 Regoliths, Elsevier, Amsterdam, pp. 275–304

977 Sherriff, J.E., Wilkinson, K.N., Adler, D.S., Arakelyan, D., Beverly, E.J., Blockley, S.P.E., Gasparyan, B., Mark,
978 D.F., Meliksetian, K., Nahapetyan, S., Preece, K.J., 2019. Pleistocene volcanism and the geomorphological
979 record of the Hrazdan valley, central Armenia: linking landscape dynamics and the Palaeolithic
980 record. *Quaternary Science Reviews*, 226, p.105994.

981 Slimak, L., Kuhn, S.L., Roche, H., Mouralis, D., Buitenhuis, H., Balkan-Atlı, N., Binder, D., Kuzucuoğlu, C. and
982 Guillou, H., 2008. Kaletepe Deresi 3 (Turkey): Archaeological evidence for early human settlement in Central
983 Anatolia. *Journal of Human Evolution,* 54 (1), pp.99-111.
984
985 Sosson, M., Rolland, Y., Müller, C., Danelian, T., Melkonyan, R., Kekelia, S., Adamia, S., Babazadeh, V.,
986 Kangarli, T., Avagyan, A., Galoyan, G., 2010. Subductions, obduction and collision in the Lesser Caucasus
987 (Armenia, Azerbaijan, Georgia), new insights. *Geological Society, London, Special Publications*, 340 (1),
988 pp.329-352.

989 Spaulding, S.A., Bishop, I.W., Edlund, M.B., Lee, S., Furey, P., Jovanovska, E. and Potapova, M. 2020. Diatoms
990 of North America. URL https://diatoms.org/ (accessed 16.08.20).

991 Stewart, M., Clark-Wilson, R., Breeze, P.S., Janulis, K., Candy, I., Armitage, S.J., Ryves, D.B., Louys, J., Duval,
992 M., Price, G.J., Cuthbertson, P., Bernal, M.A., Drake, N.A., Alsharekh, A.M., Zahrani, B., Al-Omari, A., Roberts,
993 P., Groucutt, H.S., Petraglia, M.D., 2020. Human footprints provide snapshot of last interglacial ecology in the
994 Arabian interior. *Science Advances*, 6 (38), eaba8940.

995 Stoops, G., Marcelino, V. and Mees, F. eds., 2018. *Interpretation of micromorphological features of soils and*
996 *regoliths*. Elsevier.

997 Stow, D.A. and Bowen, A.J., 1980. A physical model for the transport and sorting of fine-grained sediment by
998 turbidity currents. *Sedimentology*, 27 (1), pp.31-46.

999 Suchodoletz, H. von, Gärtner, A., Zielhofer, C., Faust. D. .2018. Eemian and post-Eemian fluvial dynamics in
1000 the Lesser Caucasus. *Quaternary Science Reviews,* 191, 189-203.

1001 Sumita, M. and Schmincke, H.U. 2013b. Impact of volcanism on the evolution of Lake Van I: evolution of
1002 explosive volcanism of Nemrut Volcano (eastern Anatolia) during the past> 400,000 years. *Bulletin of*
1003 *volcanology*, 75, 714.

1004 Sumita, M. and Schmincke, H.U. 2013b. Impact of volcanism on the evolution of Lake Van II: temporal
1005 evolution of explosive volcanism of Nemrut Volcano (eastern Anatolia) during the past ca. 0.4 Ma. *Journal of*
1006 *Volcanology and Geothermal Research*, 253 15-34.

Telford, R.J., Barker, P., Metcalfe, S. and Newton, A., 2004. Lacustrine responses to tephra deposition: examples from Mexico. *Quaternary Science Reviews*, 23 (23-24), pp.2337-2353.

Tomlinson, E. L., Smith, V. C., Albert, P. G., Aydar, E., Civetta, L., Cioni, R., Orsi, G. 2015. The major and trace element glass compositions of the productive Mediterranean volcanic sources: tools for correlating distal tephra layers in and around Europe*. Quaternary Science Reviews*, 118, 48-66.

Trigui, Y., Wolf, D., Sahakyan, L., Hovakimyan, H., Sahakyan, K., Zech, R., Fuchs, M., Wolpert, T., Zech, M., Faust, D. 2019. First calibration and application of leaf wax n-alkane biomarkers in loess-paleosol sequences and modern plants and soils in *Armenia*. Geosciences 9, 263.

Tushabramishvili, N., Pleurdeau, D., Moncel, M.-H., Agapishvili, T., Vekua, A., Bukhsianidze, M., Maureille, B., Muskhelishvili, A., Mshvildadze, M., Kapanadze, N., Lordkipanidze, D., 2012. Human remains from a new Upper Pleistocene sequence in Bondi Cave (Western Georgia). *Journal of Human Evolution*, 62, 179–185.

Tryon, C. A., Logan, M. A. V., Mouralis, D., Kuhn, S., Slimak, L.,Balkan-Atlı, N. 2009. Building a tephrostratigraphic framework for the Paleolithic of central Anatolia, Turkey. J*ournal of Archaeological Science*, 36 (3), 637-652.

Van den Bogaard, C., Schmincke, H.U., 2002. Linking the North Atlantic to central Europe: a high-resolution Holocene tephrochronological record from northern Germany. *Journal of Quaternary Science,* 17 (1), pp.3-20.

Winder, M., Hunter, D.A., 2008. Temporal organization of phytoplankton communities linked to physical forcing. *Oecologia* 156, 179–192.

Wolin, J. A., Duthie, H. C. 1999. Diatoms as indicators of water level changes in freshwater lakes. In Stoermer, E. F., J. P. Smol (eds), The Diatoms: Application for the Environmental and Earth Sciences. University Press, Cambridge: 183–202.

Wolf, D., Baumgart, P., Meszner, S., Fülling, A., Haubold, F., Sahakyan, L., Meliksetyan, K., Faust, D.,. 2016. Loess in Armenia – stratigraphic findings and palaeoenvironmental indications. *Proceedings of the Geologists'* Association ,127, 29–39.

Yılmaz, Y., Güner, Y. and Şaroğlu, F. 1998. Geology of the Quaternary volcanic centres of the East Anatolia. *Journal of Volcanology and Geothermal Research* 85, 173-210.

Zehetner, F., Miller, W.P. and West, L.T., 2003. Pedogenesis of volcanic ash soils in Andean Ecuador. *Soil Science Society of America Journal*, 67 (6), pp.1797-1809.

Figure captions

Figure 1. Location map. A) Regional map showing location of the southern Caucasus (as defined by Bailey, 1989) and positions of main volcanic regions and major lakes in the region. Blue box represents the location of (B). B) Map of the Hrazdan basin. Extent of the Quaternary volcanic deposits and main volcanic centres are highlighted. Blue box represents the location of (C). C) Satellite imagery showing the locations of BF1 and NG1 (imagery from Google Earth [2021]).

Figure 2. Site photographs. A) Overview of the BF1 section. Blue box indicates the position of (B). B) Detail of BF1-1 to BF1-8. Shown is the location of the contiguous sampling column for sedimentology, geochemistry, diatom analysis and tephrostratigraphy. Position of micromorphology samples are shown in Figure 3.

Figure 3. Summary of bulk sedimentology and tephrostratigraphy of BF1-1 to BF1-8. Shown are % >2mm fraction, low-frequency mass-specific magnetic susceptibility (on Log_{10} scale), median particle size (D_{50} µm on Log_{10} scale) and % clay (dark grey), %silt (medium grey) and %sand (light grey). Positions of micromorphological samples (MM) are also shown. Glass shard counts are shown per g/ dry weight. Red arrows and text represent levels selected for geochemical analysis.

Figure 4. Particle size distribution of BF1- to BF1-8. A) Cumulative frequency distribution for average particle size for each unit, B) XY plot showing mean particle size against sorting (calculated following method of Folk and Ward (1957))

Figure 5. Photomicrographs of key micromorphological features of the BF1 sequence. A) Massive microstructure of BF1-1 showing the presence of Fe/Mn mottling (Fe/Mn) of the groundmass and Fe/Mn hypocoatings (Fe/Mn Hyp.) of voids. PPL. B) Laminated microstructure of BF1-2 with high volume of volcanic glass and an outsized rhyolite (Rhy.) fragment. Lam. denotes a single lamination. PPL. C) BF1-2/BF1-3 contact with Fe/Mn quasicoatings (Fe Qc) around glass shards in BF1-2. A high abundance of scoria fragments is present in BF1-3. PPL. D) Laminated microstructure of BF1-4. Lam. denotes a single lamination. Groundmass is principally volcanic glass with larger glass shards and pumice fragments present. PPL. E) Upper surface of BF1-5. Clay and Fe quasi coatings (Clay & Fe Qc) of volcanic material present with high abundance of clay (Clay) evident at the contact with BF1-6. Volcanic glass (Glass) and organic fragments (Org.) present XPL. F) Higher magnification of BF1-4 contact showing stained organic material (Org.), altered (Alt. glass) and pristine volcanic glass and Fe/Mn mottling (Fe/Mn) of the groundmass. PPL. G) Massive microstructure of BF1-6 showing the presence of algal material (Algal mat.) and rounded grains of quartz/feldspar (Ro. grain). H) High magnification image of BF1-8 showing diatom rich groundmass (Diatom GM). Pennate, centric and acicular forms are present. Rounded grains of quartz/feldspar (Ro. grain) are also evident in the groundmass. PPL.

Figure 6. Summary of PCA results for the BF1 pXRF data. A) PCA biplot of selected elemental data and sedimentological parameters. Colour coding of elements based on their relative contribution to principal components, B) PCA biplot of BF1 stratigraphic units.

Figure 7. Ratios of selected elements (SI/Al, Si/Ti, Si/K, Zr/Al, V/Cr) through the BF1 sequence.

Figure 8. Selected chemical plots illustrating non-normalised major element glass chemistry of Bird Farm visible ashes and cryptotephra. The Bird Farm sequence is dominated by glass shards of an indistinguishable high-K calc-alkaline rhyolitic signature. These are likely of local origin and can be tentatively correlated to the Gutansar volcano located within the proximal GVM, despite some similarities to centres in the CAVP. (A) Total Alkali Silica classification based on normalised data (Le Bas et al., 1986), (B) SiO_2 vs. K_2O based on non-normalised data (Peccerillo and Taylor 1976). Comparative data derived from Slimak et al. (2008); Tyron et al. (2009); Schmitt et al. (2011); Tomlinson et al. (2015); Kandel et al. (2017); Malinsky-Buller et al. (2021) and authors unpublished data. Error bars represent 2 SD of replicate analyses of Lipari (n=47; plots A-E) and BCR2g (n=53; plots F-G) glass standards.

Figure 9. Summary diatom assemblage data for BF1-6 to BF1-8. Shown are the principal planktonic and benthic data, diatom concentration and axis 1 scores of the PCA.

Figure 10. Schematic showing hypothesised correlations of a) the BF1 and NG1 (Adler et al., 2014) sequence, and b) BF1 and NG1 with the global marine isotope stratigraphy (LR04; Lisecki and Raymo, 2004) and Lake Van arboreal pollen record (Litt et al., 2014). Upper NG1 stratigraphy (Units 1-4) based primarily on that

reported by Adler et al., 2014. The lower stratigraphy (Units 5g-9e) is based on more recent excavations at NG1 (Adler and Wilkinson, unpublished). Lava cobbles with silt-clay interstitial fill (Units 9a-9e) in the NG1 sequence are interpreted to represent the lacustrine facies. For both BF1 and NG1 the principal fluvial, lacustrine, pedogenic and volcanic facies are highlighted in (a) and correlated to the regional stratigraphies in (b). As described in the main text, we hypothesise that the upper fluvial and pedogenic facies in BF1 (BF1-9) are lateral equivalents to the upper fluvial and pedogenic facies at NG1 (Units 2-5) and are likely correlated to MIS 9e. The underlying lacustrine, volcanic and fluvial facies at both sites were, therefore, likely deposited during the interval 440 – 320 ka (MIS 11- MIS 10) on the basis of the $^{39}Ar/^{40}Ar$ dating of the lava flow (HGW-IV) that forms the base of the NG1 sequence.

Supplementary information 1 (S1). Tephra chemistry raw datasets, summary table and standards data.

Supplementary information 2 (S2). Diatom concentrations and raw counts

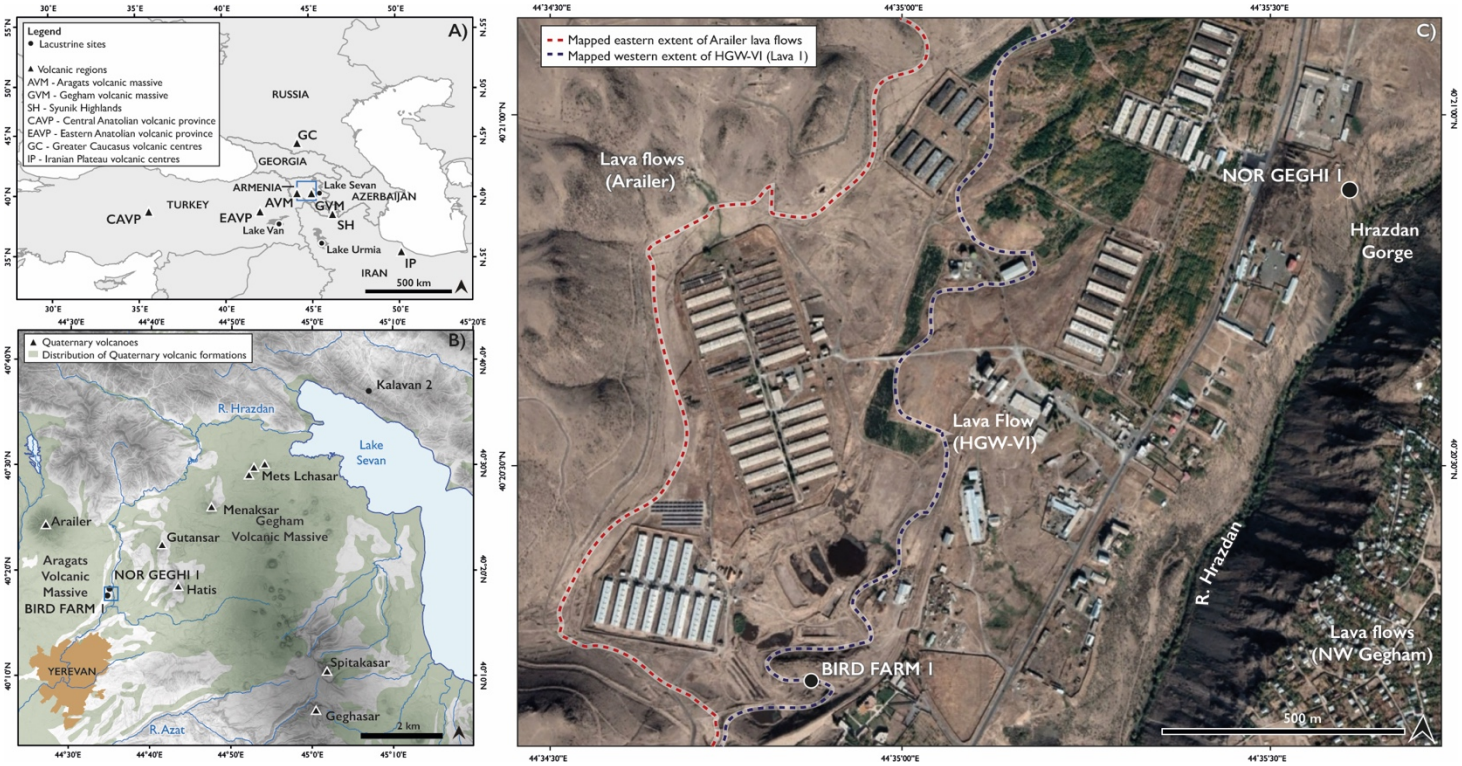

Figure 1. Location map. A) Regional map showing location of the Armenian Highlands and the southern Caucasus (as defined by Bailey, 1989) and positions of main volcanic regions and major lakes in the region. Blue box represents the location of (B). B) Map of the Hrazdan basin. Extent of the Quaternary volcanic deposits and main volcanic centres are highlighted. Blue box represents the location of (C). C) Satellite imagery showing the locations of BF1 and NG1 (imagery from Google Earth [2021]).

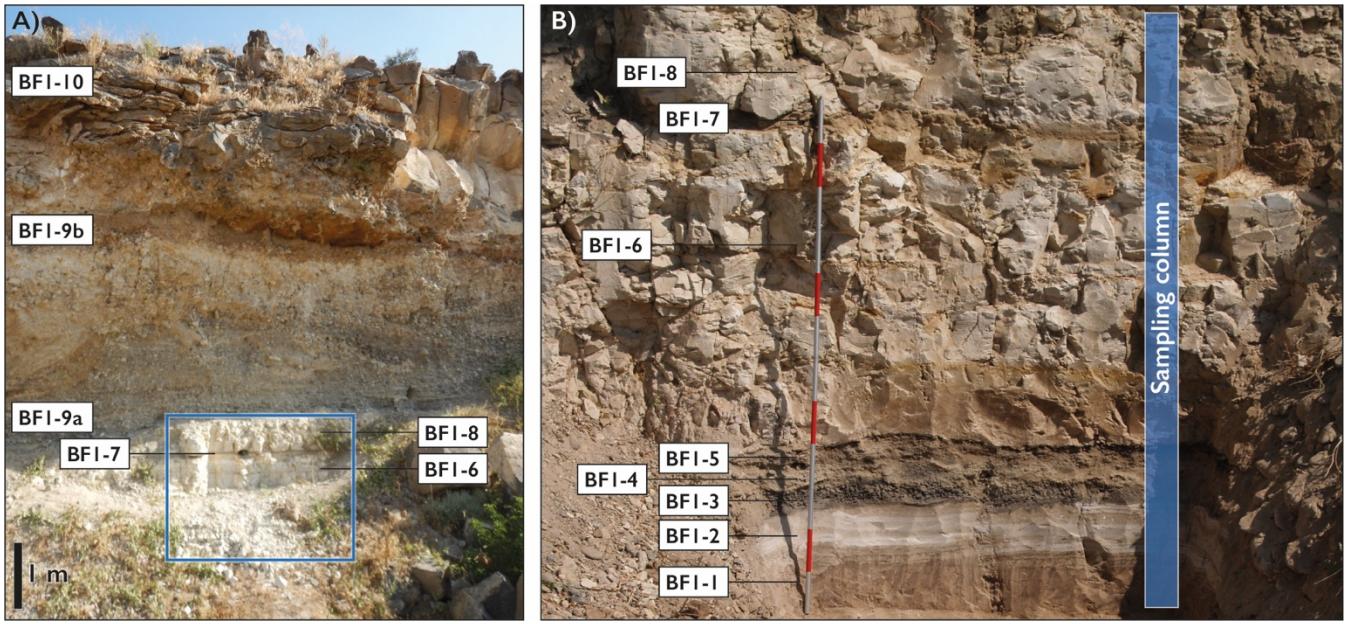

Figure 2. Site photographs. A) Overview of the BF1 section. Blue box indicates the position of (B). B) Detail of BF1-1 to BF1-8. Shown is the location of the contiguous sampling column for sedimentology, geochemistry, diatom analysis and tephrostratigraphy. Position of micromorphology samples are shown in Figure 3.

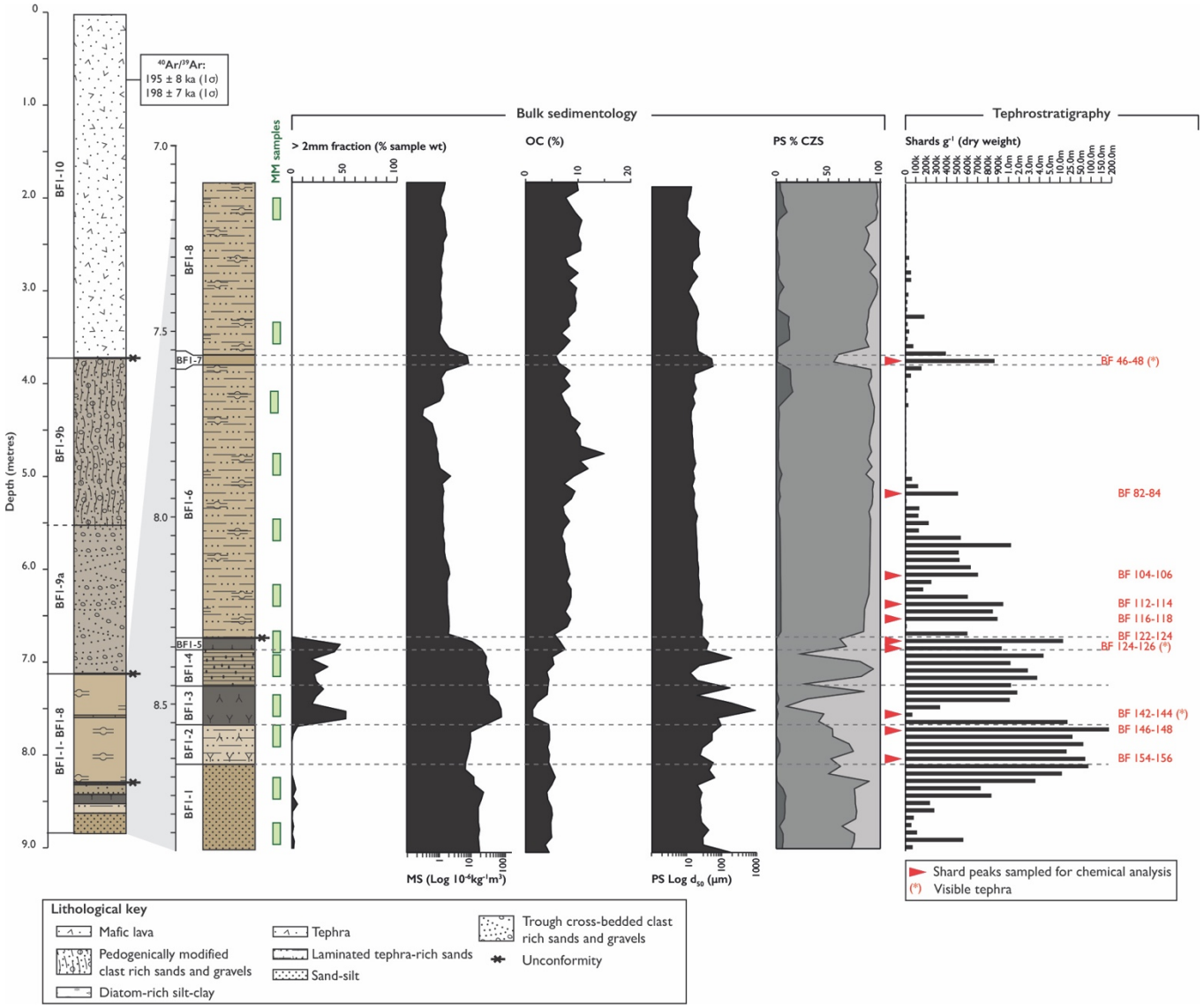
Depth (metres)
$^{40}Ar/^{39}Ar$:
195 ± 8 ka (1σ)
198 ± 7 ka (1σ)
BFI-10
BFI-9b
BFI-9a
BFI-1- BFI-8
BFI-8
BFI-7
BFI-6
BFI-5
BFI-4
BFI-3
BFI-2
BFI-1
MM samples
Bulk sedimentology
> 2mm fraction (% sample wt)
OC (%)
PS % CZS
MS (Log $10^{-5}kg^{-1}m^3$)
PS Log d_{50} (μm)
Tephrostratigraphy
Shards g^{-1} (dry weight)
BF 46-48 (*)
BF 82-84
BF 104-106
BF 112-114
BF 116-118
BF 122-124
BF 124-126 (*)
BF 142-144 (*)
BF 146-148
BF 154-156
Shard peaks sampled for chemical analysis
(*) Visible tephra
Lithological key
Mafic lava
Pedogenically modified clast rich sands and gravels
Diatom-rich silt-clay
Tephra
Laminated tephra-rich sands
Sand-silt
Trough cross-bedded clast rich sands and gravels
Unconformity

Figure 3. Summary of bulk sedimentology and tephrostratigraphy of BF1-1 to BF1-8. Shown are % >2mm fraction, low-frequency mass-specific magnetic susceptibility (on Log_{10} scale), median particle size (D_{50} µm on Log_{10} scale) and % clay (dark grey), %silt (medium grey) and %sand (light grey). Positions of micromorphological samples (MM) are also shown. Glass shard counts are shown per g/ dry weight. Red arrows and text represent levels selected for geochemical analysis.

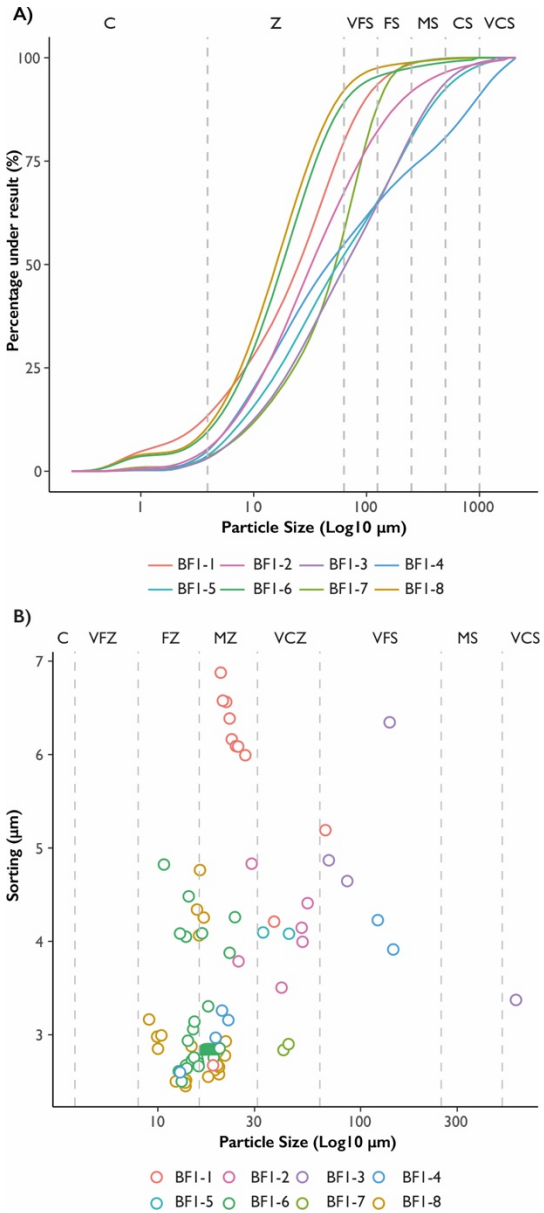
A)
C
Z
VFS
FS
MS
CS
VCS
100
75
50
25
0
Percentage under result (%)
1
10
100
1000
Particle Size (Log10 µm)
BF1-1
BF1-2
BF1-3
BF1-4
BF1-5
BF1-6
BF1-7
BF1-8
B)
C
VFZ
FZ
MZ
VCZ
VFS
MS
VCS
7
6
5
4
3
Sorting (µm)
10
30
100
300
Particle Size (Log10 µm)
BF1-1
BF1-2
BF1-3
BF1-4
BF1-5
BF1-6
BF1-7
BF1-8

Figure 4. Particle size distribution of BF1- to BF1-8. A) Cumulative frequency distribution for average particle size for each unit, B) XY plot showing mean particle size against sorting (calculated following method of Folk and Ward (1957))

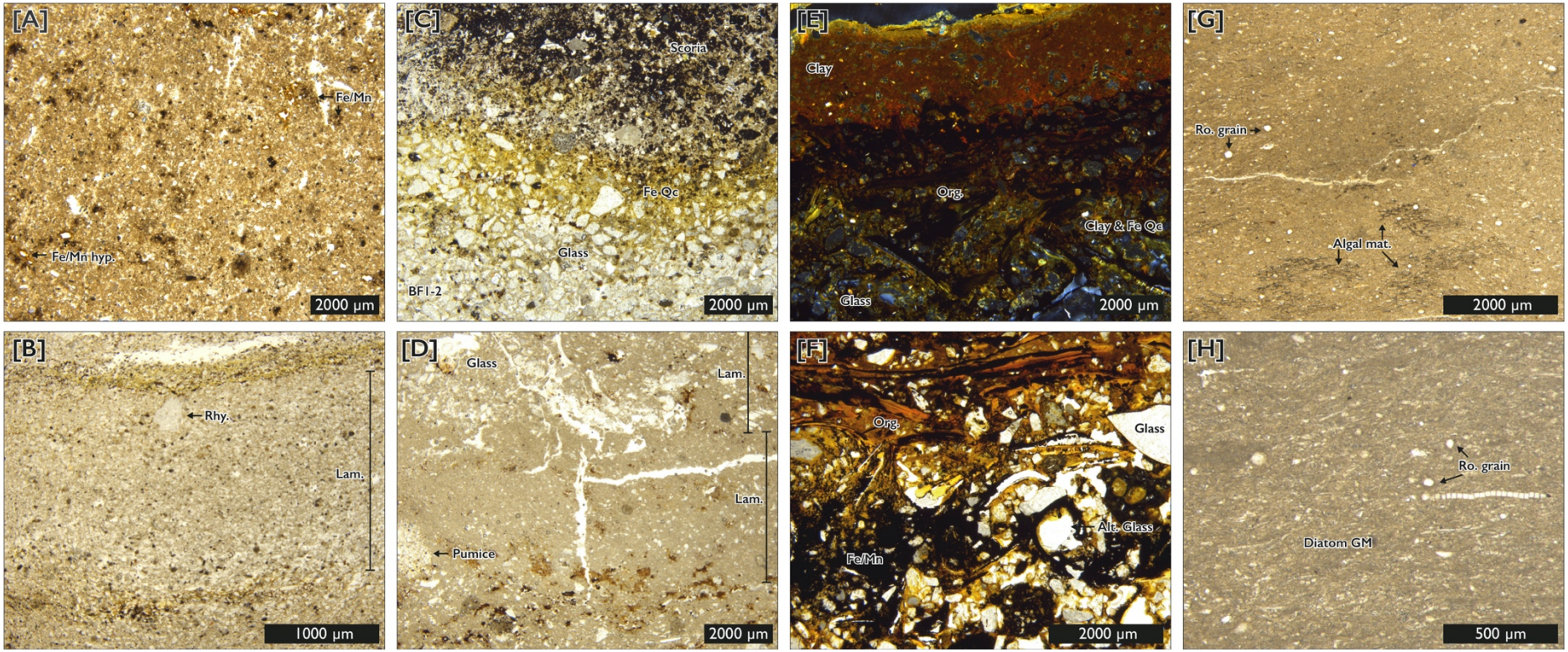

Figure 5. Photomicrographs of key micromorphological features of the BF1 sequence. A) Massive microstructure of BF1-1 showing the presence of Fe/Mn mottling (Fe/Mn) of the groundmass and Fe/Mn hypocoatings (Fe/Mn Hyp.) of voids. PPL. B) Laminated microstructure of BF1-2 with high volume of volcanic glass and an outsized rhyolite (Rhy.) fragment. Lam. denotes a single lamination. PPL. C) BF1-2/BF1-3 contact with Fe/Mn quasicoatings (Fe Qc) around glass shards in BF1-2. A high abundance of scoria fragments is present in BF1-3. PPL. D) Laminated microstructure of BF1-4. Lam. denotes a single lamination. Groundmass is principally volcanic glass with larger glass shards and pumice fragments present. PPL. E) Upper surface of BF1-5. Clay and Fe quasi coatings (Clay & Fe Qc) of volcanic material present with high abundance of clay (Clay) evident at the contact with BF1-6. Volcanic glass (Glass) and organic fragments (Org.) present XPL. F) Higher magnification of BF1-4 contact showing stained organic material (Org.), altered (Alt. glass) and pristine volcanic glass and Fe/Mn mottling (Fe/Mn) of the groundmass. PPL. G) Massive microstructure of BF1-6 showing the presence of algal material (Algal mat.) and rounded

grains of quartz/feldspar (Ro. grain). H) High magnification image of BF1-8 showing diatom rich groundmass (Diatom GM). Pennate, centric and acicular forms are present. Rounded grains of quartz/feldspar (Ro. grain) are also evident in the groundmass. PPL.

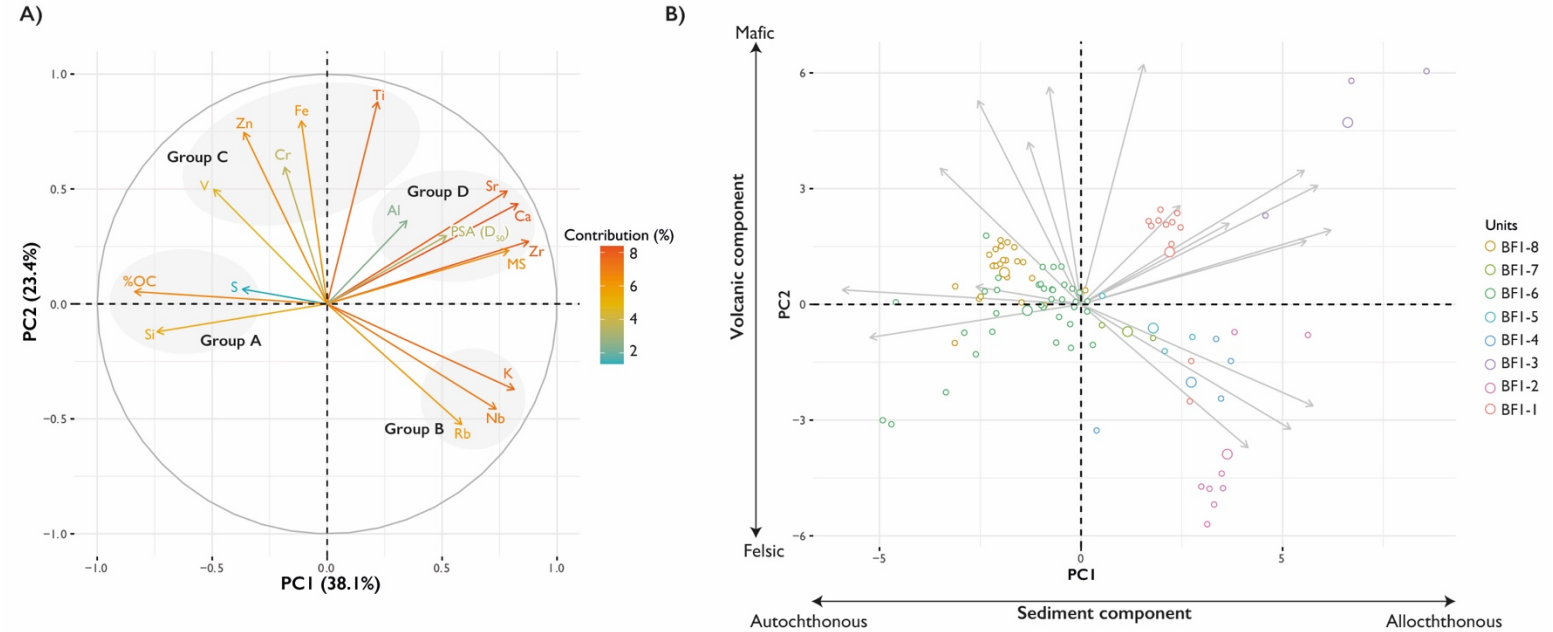

Figure 6. Summary of PCA results for the BF1 pXRF data. A) PCA biplot of selected elemental data and sedimentological parameters. Colour coding of elements based on their relative contribution to principal components, B) PCA biplot of BF1 stratigraphic units.

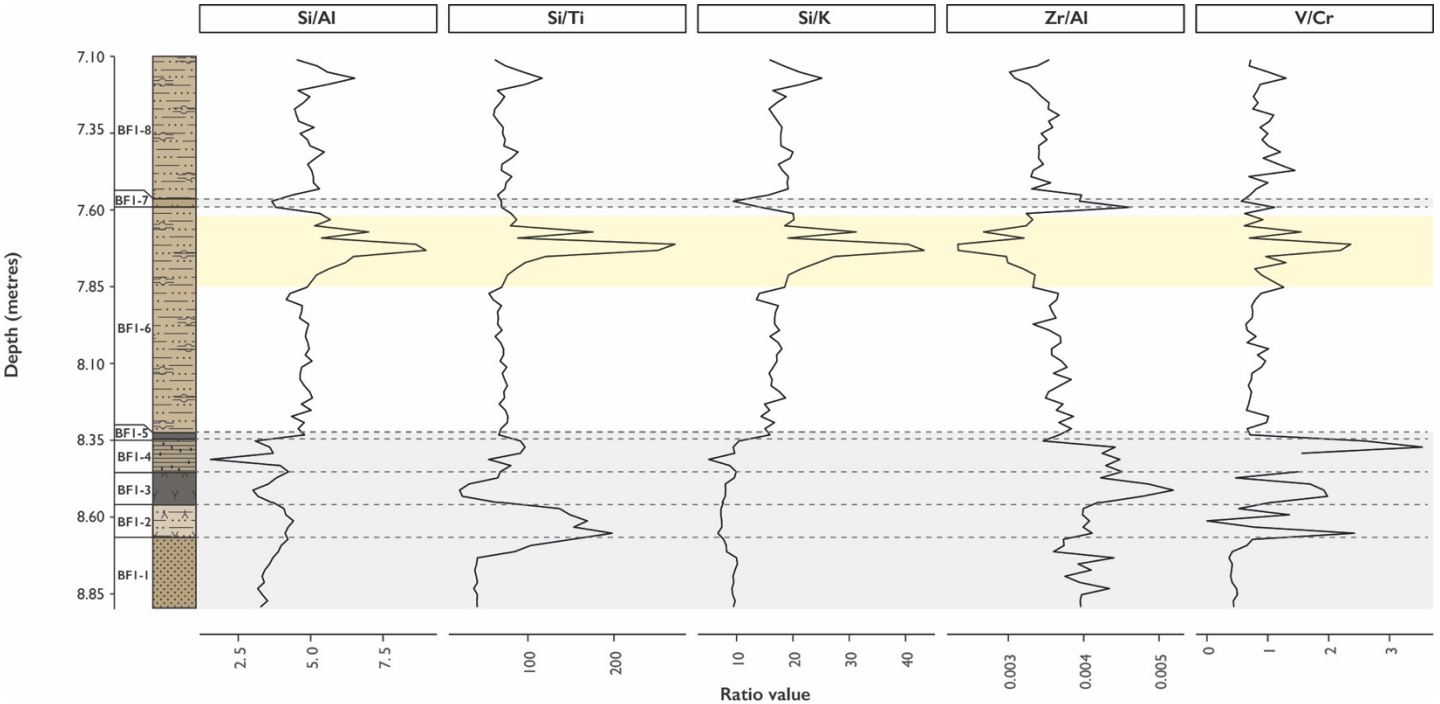

Figure 7. Ratios of selected elements (SI/Al, Si/Ti, Si/K, Zr/Al, V/Cr) through the BF1 sequence.

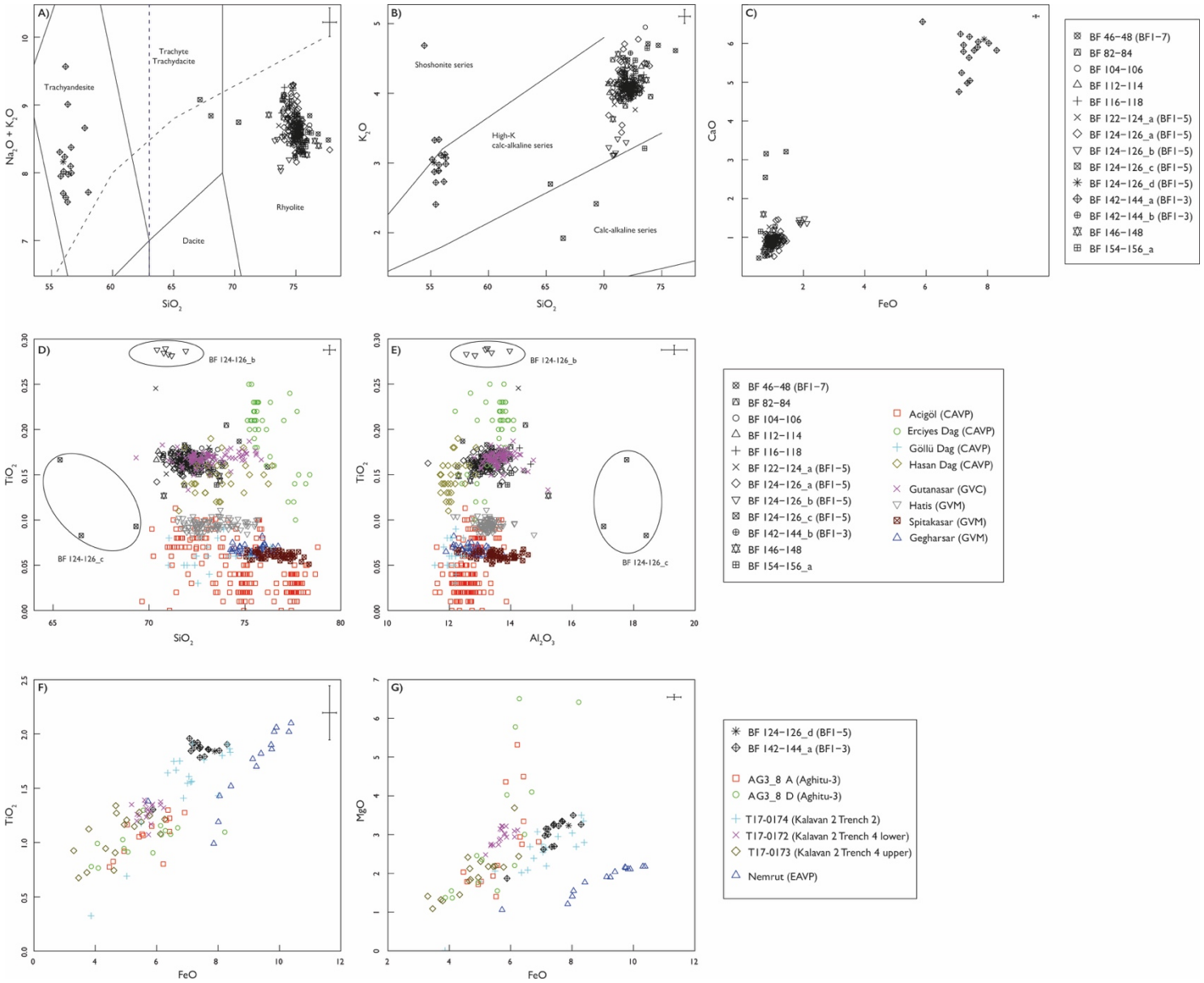
A)
Trachyte
Trachydacite
Trachyandesite
Rhyolite
Dacite
$Na_2O + K_2O$
SiO_2
B)
Shoshonite series
High-K
calc-alkaline series
Calc-alkaline series
K_2O
SiO_2
C)
CaO
FeO
BF 46–48 (BF1–7)
BF 82–84
BF 104–106
BF 112–114
BF 116–118
BF 122–124_a (BF1–5)
BF 124–126_a (BF1–5)
BF 124–126_b (BF1–5)
BF 124–126_c (BF1–5)
BF 124–126_d (BF1–5)
BF 142–144_a (BF1–3)
BF 142–144_b (BF1–3)
BF 146–148
BF 154–156_a
D)
BF 124-126_b
BF 124-126_c
TiO_2
SiO_2
E)
BF 124-126_b
BF 124-126_c
TiO_2
Al_2O_3
BF 46–48 (BF1–7)
BF 82–84
BF 104–106
BF 112–114
BF 116–118
BF 122–124_a (BF1–5)
BF 124–126_a (BF1–5)
BF 124–126_b (BF1–5)
BF 124–126_c (BF1–5)
BF 142–144_b (BF1–3)
BF 146–148
BF 154–156_a
Acigöl (CAVP)
Erciyes Dag (CAVP)
Göllü Dag (CAVP)
Hasan Dag (CAVP)
Gutanasar (GVC)
Hatis (GVM)
Spitakasar (GVM)
Gegharsar (GVM)
F)
TiO_2
FeO
G)
MgO
FeO
BF 124–126_d (BF1–5)
BF 142–144_a (BF1–3)
AG3_8 A (Aghitu-3)
AG3_8 D (Aghitu-3)
T17-0174 (Kalavan 2 Trench 2)
T17-0172 (Kalavan 2 Trench 4 lower)
T17-0173 (Kalavan 2 Trench 4 upper)
Nemrut (EAVP)

Figure 8. Selected chemical plots illustrating non-normalised major element glass chemistry of Bird Farm visible ashes and cryptotephra. The Bird Farm sequence is dominated by glass shards of an indistinguishable high-K calc-alkaline rhyolitic signature. These are likely of local origin and can be tentatively correlated to the Gutansar volcano located within the proximal GVM, despite some similarities to centres in the CAVP. (A) Total Alkali Silica classification based on normalised data (Le Bas et al., 1986), (B) SiO_2 vs. K_2O based on non-normalised data (Peccerillo and Taylor 1976). Comparative data derived from Slimak et al. (2008); Tyron et al. (2009); Schmitt et al. (2011); Tomlinson et al. (2015); Kandel et al. (2017); Malinsky-Buller et al. (2021) and authors unpublished data. Error bars represent 2 SD of replicate analyses of Lipari (n=47; plots A-E) and BCR2g (n=53; plots F-G) glass standards.

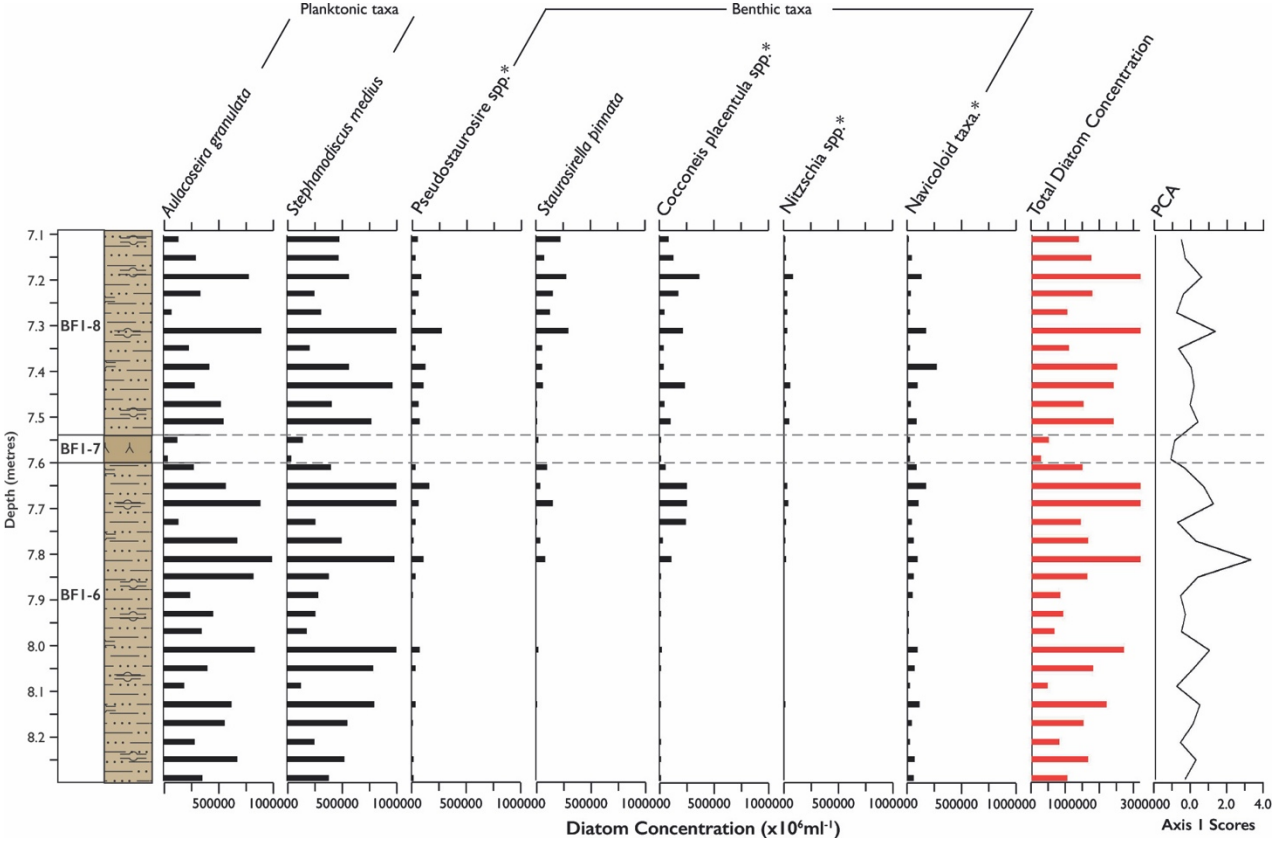

Figure 9. Summary diatom assemblage data for BF1-6 to BF1-8. Shown are the principal planktonic and benthic data, diatom concentration and axis 1 scores of the PCA.

Figure 10. Schematic showing hypothesised correlations of a) the BF1 and NG1 (Adler et al., 2014) sequence, and b) BF1 and NG1 with the global marine isotope stratigraphy (LR04; Lisecki and Raymo, 2004) and Lake Van arboreal pollen record (Litt et al., 2014). Upper NG1 stratigraphy (Units 1-4) based primarily on that reported by Adler et al., 2014. The lower stratigraphy (Units 5g-9e) is based on more recent excavations at NG1 (Adler and Wilkinson, unpublished). Lava cobbles with silt-clay interstitial fill (Units 9a-9e) in the NG1 sequence are interpreted to represent the lacustrine facies. For both BF1 and NG1 the principal fluvial, lacustrine, pedogenic and volcanic facies are highlighted in (a) and correlated to the regional stratigraphies in (b). As described in the main text, we hypothesise that the upper fluvial and pedogenic facies in BF1 (BF1-9) are lateral equivalents to the upper fluvial and pedogenic facies at NG1 (Units 2-5) and are likely correlated to MIS 9e. The underlying lacustrine, volcanic and fluvial facies at both sites were, therefore, likely deposited during the interval 440 – 320 ka (MIS 11- MIS 10) on the basis of the $^{39}Ar/^{40}Ar$ dating of the lava flow (HGW-IV) that forms the base of the NG1 sequence.

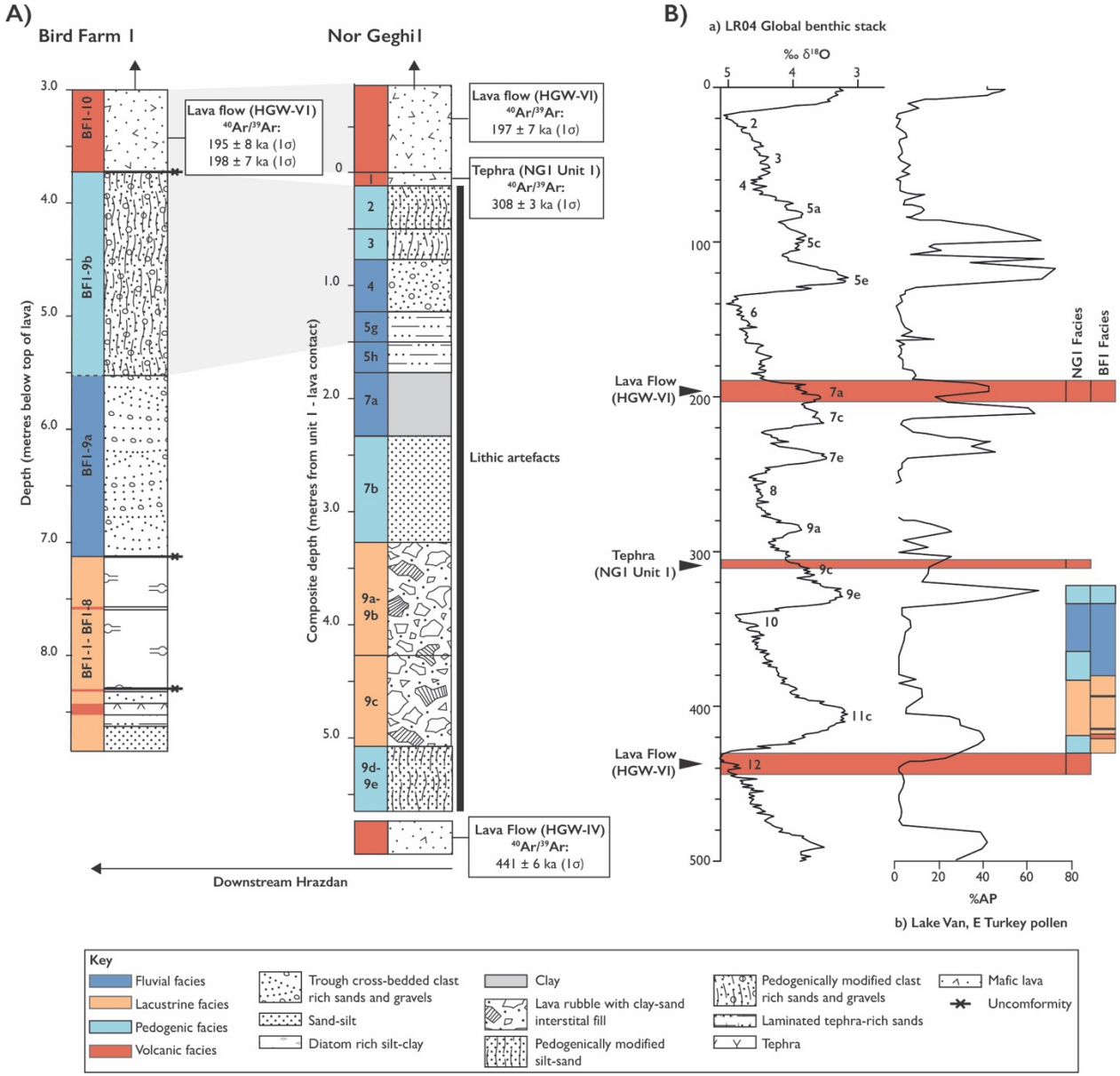
A)
Bird Farm 1
Nor Geghi1
Depth (metres below top of lava)
Composite depth (metres from unit 1 - lava contact)
BF1-10
BF1-9b
BF1-9a
BF1-1- BF1-8
1
2
3
4
5g
5h
7a
7b
9a-9b
9c
9d-9e
Lava flow (HGW-V1)
40Ar/39Ar:
195 ± 8 ka (1σ)
198 ± 7 ka (1σ)
Lava flow (HGW-VI)
40Ar/39Ar:
197 ± 7 ka (1σ)
Tephra (NG1 Unit 1)
40Ar/39Ar:
308 ± 3 ka (1σ)
Lithic artefacts
Lava Flow (HGW-IV)
40Ar/39Ar:
441 ± 6 ka (1σ)
Downstream Hrazdan
B)
a) LR04 Global benthic stack
‰ δ18O
NG1 Facies
BF1 Facies
Lava Flow (HGW-VI)
Tephra (NG1 Unit 1)
Lava Flow (HGW-VI)
%AP
b) Lake Van, E Turkey pollen
Key
Fluvial facies
Lacustrine facies
Pedogenic facies
Volcanic facies
Trough cross-bedded clast rich sands and gravels
Sand-silt
Diatom rich silt-clay
Clay
Lava rubble with clay-sand interstital fill
Pedogenically modified silt-sand
Pedogenically modified clast rich sands and gravels
Laminated tephra-rich sands
Tephra
Mafic lava
Uncomformity